Lipid-mediated regulation of SKN-1/Nrf in response to germ cell absence

Michael J. Steinbaugh[1,2], Sri Devi Narasimhan[1,2], Stacey Robida-Stubbs[1,2], Lorenza E. Moronetti Mazzeo[1,2], Jonathan M. Dreyfuss[1,3], John M. Hourihan[1,2], Prashant Raghavan[1,2], Theresa N. Operaña[1,2], Reza Esmaillie[1,2], and T. Keith Blackwell[1,2]

[1] Research Division, Joslin Diabetes Center, Boston, MA 02215, USA
[2] Department of Genetics and Harvard Stem Cell Institute, Harvard Medical School, Boston, MA 02215, USA
[3] Department of Biomedical Engineering, Boston University, Boston, MA 02215, USA

Contact: keith.blackwell@joslin.harvard.edu

Running title: Germ cell and lipid regulation of SKN-1/Nrf

Keywords: aging, germline stem cells, lipid metabolism, fatty acid signaling, proteostasis, SKN-1/Nrf

Abstract

In *C. elegans,* ablation of germline stem cells (GSCs) extends lifespan, but also increases fat accumulation and alters lipid metabolism, raising the intriguing question of how these effects might be related. Here we show that a lack of GSCs results in a broad transcriptional reprogramming, in which the conserved detoxification regulator SKN-1/Nrf increases stress resistance, proteasome activity, and longevity. SKN-1 also activates diverse lipid metabolism genes and reduces fat storage, thereby alleviating the increased fat accumulation caused by GSC absence. Surprisingly, SKN-1 is activated by signals from this fat, which appears to derive from unconsumed yolk that was produced for reproduction. We conclude that SKN-1 plays a direct role in maintaining lipid homeostasis, in which it is activated by lipids. This SKN-1 function may explain the importance of mammalian Nrf proteins in fatty liver disease, and suggests that particular endogenous or dietary lipids might promote health through SKN-1/Nrf.

Introduction

The nematode *C. elegans* has been invaluable for identifying mechanisms that slow aging and may prevent chronic disease (Kenyon, 2010). An intriguing finding that was first made in this organism is that when germline stem cells (GSCs) are ablated, mechanisms are activated in somatic tissues that protect against stress and increase lifespan (Hsin and Kenyon, 1999; Kenyon, 2010; Antebi, 2013; Hansen et al., 2013). GSC loss also increases lifespan in *D. melanogaster* (Flatt et al., 2008), and castration has been associated with longevity in men (Min et al., 2012), suggesting that this relationship might be conserved. These beneficial effects of GSC removal may have evolved to maximize reproductive fitness under adversity (Partridge et al., 2005; Kenyon, 2010). This relationship provides paradigms for how tissue non-autonomous signals influence aging (Kenyon, 2010), and how a stem cell population communicates with the "niche" that sustains it (Jones and Wagers, 2008).

In *C. elegans*, the effects of GSC absence have been studied by laser ablation of GSC precursors, which results in a complete loss of GSCs, or by analysis of genetic mutants in which GSC proliferation is inhibited so that the GSC number is very low, and mature germ cells are not formed (Hsin and Kenyon, 1999; Arantes-Oliveira et al., 2002; Kenyon, 2010). For simplicity, we will refer to each of these types of animals as GSC(-) animals. The lifespan extension seen in GSC(-) animals (GSC(-) longevity) requires the action of several conserved transcription factors in the intestine, the counterpart of the mammalian liver, digestive system, and adipose tissue (Kenyon, 2010; Antebi, 2013; Hansen et al., 2013). DAF-16/FOXO is needed for longevity from GSC ablation or reduced insulin/IGF-1 signaling (IIS), but is regulated differently by each pathway (Lin et

al., 2001; Libina et al., 2003; Kenyon, 2010). GSC(-) longevity also requires HLH-30/TFEB, PHA-4/FOXA, and the nuclear receptors DAF-12/FXR, NHR-80/HNF4, and NHR-49/PPARα (Hsin and Kenyon, 1999; Goudeau et al., 2011; Lapierre et al., 2011; O'Rourke and Ruvkun, 2013; Ratnappan et al., 2014). Under most conditions, GSC(-) longevity also depends upon a hormonal signal from the somatic gonad that activates DAF-12 (Kenyon, 2010; Antebi, 2013). Aside from the identification of mechanisms required for DAF-16 function, we understand little about how GSCs influence these transcription factors (Kenyon, 2010; Antebi, 2013).

One hallmark of GSC(-) animals is enhancement of both proteostasis and stress resistance. During aging, GSC(-) animals maintain more robust responses to thermal and proteotoxic stress (Ben-Zvi et al., 2009). They also exhibit a striking *daf-16*-dependent increase in activity of the proteasome (Vilchez et al., 2012), a multisubunit complex which degrades proteins that the ubiquitylation system has tagged for decay (Glickman and Ciechanover, 2002; Goldberg, 2003). In addition, GSC removal enhances immunity (Alper et al., 2010), and boosts oxidative stress resistance through an undetermined DAF-16-independent mechanism (Libina et al., 2003).

Another notable characteristic of GSC(-) animals is that many aspects of lipid metabolism are altered. Expression of particular fatty acid (FA) oxidation, FA desaturation, and triglyceride lipase genes is increased, as is total lipase activity (Wang et al., 2008; Goudeau et al., 2011; Lapierre et al., 2011; McCormick et al., 2012; Ratnappan et al., 2014). Given that lipid catabolism activities are elevated, it seems paradoxical that GSC(-) animals also exhibit dramatically increased fat accumulation (O'Rourke et al., 2009). Interestingly, GSC(-) longevity seems to depend upon

73 particular lipid metabolism processes. Production of the unsaturated free FA (FFA)
74 oleic acid (OA) is required (Goudeau et al., 2011), as are the triglyceride lipases LIPL-
75 4/LIPA and FARD-1/FAR2 (Wang et al., 2008; McCormick et al., 2012). It is of intense
76 interest to determine whether the fat accumulation seen with GSC ablation might derive
77 from production and storage of particular beneficial fats, or a salutary overall balance of
78 lipid metabolism that is consistent with longevity (Ackerman and Gems, 2012; Hansen
79 et al., 2013).
80 The *C. elegans* transcription factor SKN-1 controls a broad detoxification
81 response to oxidative and xenobiotic stress, and is orthologous to the mammalian
82 Nrf1/2/3 (NF-E2-related factor) proteins (An and Blackwell, 2003; Oliveira et al., 2009;
83 Park et al., 2009). SKN-1/Nrf proteins have been implicated in longevity from *C.*
84 *elegans* to rodents (An and Blackwell, 2003; Bishop and Guarente, 2007; Leiser and
85 Miller, 2010; Sykiotis and Bohmann, 2010; Steinbaugh et al., 2012; Ewald et al., 2015).
86 Recent findings raise the question of whether these transcription regulators might also
87 have important functions in lipid homeostasis. SKN-1/Nrf proteins influence expression
88 of lipid metabolism genes (Oliveira et al., 2009; Paek et al., 2012; Hayes and Dinkova-
89 Kostova, 2014; Tsujita et al., 2014), and SKN-1 has been linked to fat mobilization
90 under particular starvation or dietary conditions (Paek et al., 2012; Pang et al., 2014).
91 Mice that lack Nrf1 in the liver develop non-alcoholic fatty liver disease (NAFLD) that
92 progresses to non-alcoholic steatohepatitis (NASH), and $Nrf2^{-/-}$ mice develop NASH on
93 a high-fat diet (Xu et al., 2005; Okada et al., 2013; Tsujita et al., 2014). However,
94 reduced Nrf protein function is thought to predispose to NASH by impairing hepatic
95 stress resistance (Xu et al., 2005; Lee et al., 2013). An understanding of NAFLD is a

high priority, because its incidence is increasing as a sequella of metabolic syndrome (Cohen et al., 2011).

Here we examined the role of SKN-1 in the effects of GSC absence on lifespan, stress resistance, and lipid metabolism. Genetic inhibition of GSCs activates SKN-1, thereby increasing lifespan and stress resistance. Expression profiling revealed that GSC(-) animals upregulate stress defense, extracellular matrix, and lipid metabolism genes, in many cases dependent upon *skn-1*. SKN-1 is also required for GSC inhibition to increase proteasome activity. SKN-1 is needed for GSC(-) longevity but reduces lipid storage, arguing against the idea that GSC(-) animals simply accumulate beneficial fat. Instead, these high fat levels appear to derive from unconsumed yolk that was produced for reproduction. Unexpectedly, in GSC(-) animals SKN-1 appears to be activated by specific FA signals, defining a new mechanism of SKN-1/Nrf protein regulation and GSC-to-soma communication. This homeostatic function of SKN-1 in lipid metabolism suggests that Nrf proteins have a similar role in preventing NASH.

Results

SKN-1 promotes longevity and stress resistance in the absence of GSCs

To investigate the importance of *skn-1* in GSC(-) animals, we analyzed temperature sensitive (ts) mutations in *glp-1*/Notch, which is required for GSC proliferation (Kimble and Crittenden, 2005). *glp-1(ts)* mutants that undergo larval development at the non-permissive temperature of 25°C (GSC(-) animals) are sterile, exhibit a markedly reduced number of GSCs, and live considerably longer that WT controls (Arantes-Oliveira et al., 2002) (**Figures 1A and 1B**). By contrast, this lifespan extension was blocked in a *skn-1* mutant background (**Figures 1A and 1B**). Lack of

skn-1 also impaired lifespan extension when *glp-1(ts)* animals were downshifted to 20°C after development was complete (**Table 1**). Similar results were obtained with or without 5-fluoro-2'-deoxyuridine (FUdR), which inhibits offspring formation in the control (**Table 1**). Consistent with these findings, in an earlier experiment in which *glp-1(ts)* extended lifespan by less than 7%, *skn-1* knockdown by RNA interference (RNAi) prevented this increase (Vilchez et al., 2012). In contrast to *daf-16, skn-1* was also required for GSC inhibition to increase oxidative stress resistance (**Figures 1C-1F; Table 2**).

GSCs regulate intestinal DAF-16 and SKN-1 through different mechanisms

We investigated whether the benefits of GSC absence simply require that SKN-1 be present, or involve activation of SKN-1. SKN-1 accumulates in intestinal nuclei in response to certain stresses, or inhibition of mechanisms that include IIS, mTORC2, glycogen synthase kinase-3 (GSK-3), translation elongation, and the ubiquitin ligase WDR-23 (An and Blackwell, 2003; Tullet et al., 2008; Choe et al., 2009; Park et al., 2009; Li et al., 2011; Robida-Stubbs et al., 2012). The levels of a SKN-1::GFP (green fluorescent protein) fusion in intestinal nuclei were also notably elevated in GSC(-) animals (**Figures 2A-2B**). This was associated with increased expression of direct SKN-1 target genes, apparently through activation of their intestinal expression (**Figures 2C-2E**). The KRI-1/KRIT1 ankyrin-repeat protein and the TCER-1/TCERG1 transcription factor are required for GSC absence to induce DAF-16 nuclear accumulation and extend lifespan (Berman and Kenyon, 2006; Ghazi et al., 2009). In contrast, in GSC(-) animals SKN-1 nuclear accumulation was only partially or minimally affected by loss of *kri-1* or *tcer-1*, respectively, but was abolished by knockdown of the

142 *pmk-1*/p38 kinase (**Figures 2F and 2G**), which phosphorylates SKN-1 and under most
143 circumstances is required for SKN-1 nuclear accumulation (Inoue et al., 2005). In
144 GSC(-) animals, DAF-12 is needed for DAF-16 nuclear accumulation and activity
145 (Berman and Kenyon, 2006; Kenyon, 2010; Antebi, 2013), and induces expression of
146 the microRNAs *mir-84* and *mir-241*, which target inhibitors of DAF-16 (Shen et al.,
147 2012). In GSC(-) animals, *daf-12* knockdown only mildly affected SKN-1::GFP
148 accumulation (**Figure 2G**), and SKN-1 target gene induction was generally not impaired
149 by *daf-12* or *mir-241;mir-84* mutations (**Figure 2H**). The absence of GSCs therefore
150 activates SKN-1 in the intestine, but through a different mechanism from DAF-16.

151 **SKN-1 reprograms stress resistance and metabolism in GSC(-) animals**

152 To investigate how SKN-1 promotes longevity and stress resistance upon GSC
153 loss, we used RNA sequencing (RNA-seq) to identify genes that are (1) expressed at
154 higher levels in adult somatic tissues when germ cells are largely absent, and (2)
155 dependent upon SKN-1 (**Figure 3A**). We compared intact *glp-1(ts)* (GSC(-)) animals to
156 wild-type GSC(+) controls at the non-permissive temperature of 25**°**, analyzing day-one
157 adults in which development was complete, and performing differential expression
158 analyses on the normalized RNA-seq data for 12,595 expressed genes (**Figure 3B**).
159 We detected similar expression levels of SKN-1 upregulated targets in qRT-PCR
160 analyses of the samples used for sequencing, giving us confidence in our RNA-seq
161 results (**Figure 3–figure supplement 1A**). Moreover, in the GSC(-) gene set, the
162 canonical DAF-16 targets *mtl-1* and *sod-3* (Murphy et al., 2003; Kenyon, 2010) were
163 upregulated (**Supplementary file 1a**), and functional groups that are characteristic of
164 germline-specific genes were under-represented (**Figure 3–figure supplement 1B**).

No previous studies have globally profiled genes that are upregulated in the soma in response to germ cell loss. mRNAs that are present at higher relative levels in GSC(-) samples compared to WT would include not only those genes, but also genes that are expressed only in somatic cells, because the germline accounts for about two-thirds of all adult nuclei (Kimble and Crittenden, 2005). To gauge the maximal extent of this background, we examined mRNAs that are expressed specifically in somatic tissues. These somatic-specific mRNAs were enriched 3-4 fold in the GSC(-) samples, approximately the level predicted from the 2:1 proportion of germline to somatic nuclei (**Figure 3–figure supplement 1C**). Accordingly, if an mRNA that is not somatic-specific was present at a four-fold elevated level in GSC(-) samples, we considered this mRNA to be upregulated in the soma in response to GSC absence, although we expect that this stringent cutoff would miss many upregulated genes.

In GSC(-) animals, 1,306 and 615 genes were upregulated more than 4- and 5-fold, respectively, indicating a broad remodeling of transcription (**Figure 3–figure supplements 1D and 1E; Supplementary file 1a**). In the latter set, which is more amenable to functional annotation analysis because of its smaller size, the most prominently overrepresented category was collagen (**Figure 3C; Supplementary file 1a**). Although collagens may be expressed primarily in the soma, this overrepresentation is likely to be meaningful because of the extent to which these genes were upregulated (**Supplementary file 1a**), and because collagens are generally overrepresented in other longevity-associated gene sets, with certain collagens being critical for lifespan extension (Ewald et al., 2015). Also notably upregulated in GSC(-) animals were genes involved in detoxification, immunity (C-type lectin and galectin), and

188 metabolism, particularly FA oxidation and other lipid metabolism processes (**Figure 3C;**
189 **Supplementary file 1a**).

190 We used RNAi to investigate the contribution of *skn-1* to gene expression in
191 GSC(-) animals (**Figure 3A**). A previous microarray analysis of *skn-1* RNAi-treated L4
192 larvae at 20°C found that in the absence of acute stress, SKN-1 upregulates genes
193 involved in processes that include detoxification, lipid metabolism, immunity, and
194 proteostasis (Oliveira et al., 2009; Li et al., 2011). Similar processes were prominent in
195 the sets of genes for which *skn-1* RNAi reduced expression at 25°C in day-one WT
196 adults ("SKN-1-upregulated in WT genes"; ≥ 33% reduction, $P < 0.05$) (**Supplementary**
197 **file 1b**), or day-one GSC(-) animals ("SKN-1-upregulated in GSC(-) genes"; ≥ 33%
198 reduction, $P < 0.05$) (**Supplementary file 1c**). Our finding that SKN-1 nuclear
199 occupancy is increased in GSC(-) animals (**Figure 2**) predicts that GSC inhibition would
200 induce SKN-1 to activate genes. Accordingly, *skn-1* RNAi reduced expression of 87
201 genes that were upregulated at least four-fold in *glp-1(ts)* compared to WT (**Figures 3D**
202 **and 3E; Supplementary file 1d**). This number probably underestimates the full
203 contribution of SKN-1, because RNAi only partially reduces its activity. In addition to
204 detoxification and lipid metabolism genes, these 87 genes included many involved in
205 extracellular matrices (ECMs), as expected from the *skn-1*-dependence of many ECM
206 genes that are upregulated in other long-lived *C. elegans* (Ewald et al., 2015). Many of
207 these *skn-1*-dependent GSC(-) genes appear to be direct SKN-1 targets, as predicted
208 by presence of SKN-1 binding sites in their upstream regions, and direct binding of
209 SKN-1 in genome-wide chromatin immunoprecipitation (ChIP) surveys (**Supplementary**
210 **file 1d**). In summary, SKN-1 upregulates numerous genes that are associated with

phenotypes seen in GSC-ablated animals, including increased stress resistance, immunity, and longevity, as well as alterations in lipid metabolism.

SKN-1 increases proteasome activity in response to GSC loss

A previous RNAi experiment suggested that SKN-1 is dispensable for the elevated proteasome activity seen in GSC(-) animals (Vilchez et al., 2012). We reexamined this question because SKN-1 maintains proteasome gene expression and intestinal proteasome activity in WT *C. elegans* (Li et al., 2011), and because proteasome genes were prominent in the SKN-1-upregulated GSC(-) gene set (**Supplementary file 1c**). The proteasome holocomplex consists of a 20S barrel-like structure in which proteins are degraded, and a 19S regulatory cap that directs ubiquitylated proteins into this structure (Glickman and Ciechanover, 2002; Goldberg, 2003). In general, and consistent with previous findings (Vilchez et al., 2012), the relative levels of proteasome subunit mRNAs were lower in GSC(-) animals (**Figure 4–figure supplement 1A**), possibly because of the lack of germ cells. In both WT and GSC(-) animals, *skn-1* knockdown comparably decreased expression of 19S and 20S proteasome subunit genes (**Figure 4A and Figure 4–figure supplement 1A**), the majority of which appear to be direct transcriptional targets of SKN-1 (**Figure 4B**). As these findings would predict, in GSC(-) animals lack of *skn-1* dramatically reduced proteasome activity at days one and five of adulthood (**Figures 4C, 4D, and Figure 4–figure supplements 1B-1G)**. It is possible that in the earlier analysis (Vilchez et al., 2012), RNAi might not have inhibited *skn-1* expression sufficiently to detect its importance for proteasome activity in GSC(-) animals.

The increased proteasome activity of GSC(-) animals is thought to derive from DAF-16-dependent transcriptional upregulation of the RPN-6.1/PSMD11 subunit, which connects the 19S and 20S proteasome particles (Vilchez et al., 2012). *rpn-6.1* appears to be unique among proteasome subunit genes, in that its mRNA levels are proportionally higher in GSC(-) animals (Vilchez et al., 2012) (**Figure 4E**). *skn-1* was required for this increased *rpn-6.1* expression (**Figure 4E**), and binding site and ChIP studies suggested that *rpn-6.1* is upregulated directly by both SKN-1 and DAF-16 (**Figure 4F**). We conclude that by promoting expression of multiple proteasome subunit genes, including *rpn-6.1*, SKN-1 plays a central role in the increased proteasome activity that results from GSC loss.

SKN-1 regulates lipid metabolism

Genetic GSC inhibition increased expression of lipid metabolism genes that represent a wide range of processes, including FFA formation from triglyceride lipolysis, as well as FA oxidation, desaturation, and elongation (**Figure 5A; Supplementary file 1a**). Many of these genes were also upregulated by SKN-1 (**Figure 5A; Supplementary files 1a-1c**). Of particular note, the high-confidence GSC(-) and SKN-1-upregulated gene set included the conserved lysosomal triglyceride lipase *lipl-3*, which increases *C. elegans* lifespan when overexpressed, and is normally induced by fasting (O'Rourke and Ruvkun, 2013). This gene set also included the FA oxidation genes *acs*-10 (acyl-CoA synthetase), *cpt-3* (carnitine palmitoyltransferase), and *ech-9* (enoyl-CoA hydratase) (**Figure 5A; Supplementary file 1d**). This suggested that SKN-1 might have a major role in lipid metabolism, and how it is influenced by GSC absence.

Given that SKN-1 increases both lifespan and stress resistance in GSC(-) animals, its effects on lipid metabolism should also be beneficial. If the elevated fat storage in GSC(-) animals reflects simply elevated production and storage of "good" lipids, we might expect *skn-1* to support this fat production. We investigated whether SKN-1 affects fat storage in WT and GSC(-) animals by oil red O (ORO) staining of fixed animals, a method that reliably indicates fat accumulation (O'Rourke et al., 2009). Remarkably, ablation of *skn-1* by either mutation or RNAi significantly increased lipid levels in either WT or GSC(-) day-one adults, so that *glp-1(ts);skn-1(-)* animals exhibited markedly high levels of ORO staining (**Figures 5B, 5C, and Figure 5–figure supplements 1A, 1B**). As an independent method of assessing fat accumulation in the intestine, we examined levels of the predicted short-chain FA dehydrogenase DHS-3 (Zhang et al., 2012). Proteomic and microscopy analyses have shown that DHS-3 localizes almost exclusively to intestinal lipid droplets (**Figure 5–figure supplement 2A**), and marks the vast majority of these lipid droplets *in vivo* (Zhang et al., 2012; Na et al., 2015). Consistent with ORO staining, lack of *skn-1* increased accumulation of a DHS-3::GFP (green fluorescent protein) fusion in the intestine in WT and GSC(-) animals, without affecting expression of the *dhs-3* mRNA (**Figure 5–figure supplements 2B, 2C, and 3**). An analysis of total triglyceride levels also indicated that SKN-1 reduces the overall level of fat accumulation (**Figure 5–figure supplement 2D**).

DAF-16 increases lipid accumulation in response to reduced IIS, and influences expression of some lipid metabolism genes in response to GSC removal (Wang et al., 2008; McCormick et al., 2012). However, consistent with a previous study (O'Rourke et al., 2009), we found that loss of *daf-16* did not substantially affect overall fat storage in

GSC(-) animals (**Figures 5D, 5E, and Figure 5–figure supplement 1C)**. Together, our data indicate that SKN-1 is required to prevent excess fat accumulation under normal feeding conditions, and that SKN-1 but not DAF-16 reduces the lipid load that accumulates in response to GSC loss.

GSC loss activates SKN-1 through lipid signaling

Given that SKN-1 inhibits fat storage, we considered whether the SKN-1 activation seen in GSC(-) animals might be triggered by lipid accumulation. It is possible that GSC loss simply increases production of certain fats. However, GSC ablation or inhibition prevents formation of oocytes, which endocytose lipid-rich yolk that is synthesized in the intestine (Grant and Hirsh, 1999). Fat storage might therefore be increased indirectly by GSC loss, through accumulation of unused yolk lipids. We tested a key prediction of this model by examining yolk accumulation and distribution, which can be visualized with GFP-tagged vitellogenin (YP170/VIT-2::GFP), a major yolk lipoprotein (Grant and Hirsh, 1999). VIT-2::GFP was visible primarily in oocytes and embryos in WT day-one adults, but accumulated to extremely high levels throughout the body cavity in the absence of GSCs (**Figures 6A, 6B, and Figure 6–figure supplement 1**). Apparently, yolk production was not slowed sufficiently to compensate for the lack of gametogenesis. The failure to consume yolk-associated lipid could account for the increase in overall fat storage seen in GSC(-) animals.

We investigated whether accumulation of yolk-associated lipids might induce SKN-1 to mount a protective response. Supporting this idea, when the oocyte-specific yolk receptor *rme-2* is knocked down, yolk accumulates to high levels (Grant and Hirsh, 1999), and in the intestine SKN-1 accumulates in nuclei and its target gene *gst-4* is

activated (**Figures 6C-6F**). Additionally, *rme-2* RNAi increased stress resistance in a *skn-1*-dependent manner (**Figure 6G and Table 2**). When *de novo* lipogenesis was prevented by knockdown of the SREBP1 ortholog *sbp-1* (Yang et al., 2006), SKN-1::GFP failed to accumulate in intestinal nuclei in response to GSC inhibition (**Figures 6H, 6I**), but not oxidative stress (**Figure 6–figure supplement 2A**) or reduced IIS (*daf-2* mutants, **Figure 6–figure supplement 2B**). The *sbp-1* lipogenesis defect can be rescued by supplementation with 600 μM OA (Yang et al., 2006), which is the most abundant FA in olive oil, chicken egg yolk, and human adipose tissue (National Research Council, 1976; Kokatnur et al., 1979). In *C. elegans*, the abundance of OA is increased in GSC(-) animals, and its synthesis by the FA desaturases FAT-6 and FAT-7 (SCD orthologs) is required for GSC(-) lifespan extension (Goudeau et al., 2011). *fat-6/7* were also required for SKN-1 to accumulate in nuclei after GSC inhibition (**Figure 6J**). Moreover, in GSC(-) animals subjected to *sbp-1* RNAi, SKN-1 nuclear accumulation was fully restored by OA supplementation (**Figures 6H and 6I**). Consistent with their importance for SKN-1 function, *sbp-1* and *fat-6/7* were required for GSC absence to increase stress resistance (**Figure 6–figure supplement 3**).

Together, our data suggest that certain unsaturated lipids are required for SKN-1 to be activated in response to GSC loss, but not necessarily by other stimuli, and therefore that lipid accumulation *per se* might activate SKN-1. Accordingly, feeding of either OA or coconut oil (CO) activated *gst-4* in WT animals in a *skn-1*-dependent manner without impairing development or reproduction (**Figure 6–figure supplements 2C-2E**). Under these conditions, CO feeding provided OA (300 μM with 0.1% CO) along with multiple saturated fatty acids. CO feeding strongly induced nuclear

accumulation of SKN-1 but not DAF-16 (**Figure 6–figure supplements 2F and 2G**), and *sbp-1* RNAi did not impair DAF-16 nuclear accumulation in GSC(-) animals (**Figure 6–figure supplements 2H and 2I**), supporting the notion that GSCs regulate SKN-1 and DAF-16 differently.

The lipid overload that results from reproductive failure might induce stress that activates SKN-1. Oxidative stress induced by sodium arsenite (AS) robustly activates the p38/PMK-1 kinase through phosphorylation, leading in turn to SKN-1 activation (Inoue et al., 2005). GSC loss induced SKN-1 nuclear accumulation at least as dramatically as AS treatment (**Figure 2B and Figure 6–figure supplement 2A**) but did not detectably increase PMK-1/p38 activity (**Figure 6–figure supplement 2J**), suggesting that any stress arising from the lack of GSCs might not be sufficient on its own to explain SKN-1 activation.

By breaking down triglycerides, the lysosomal lipases LIPL-1/3 and LIPL-4 enable production of specific unsaturated FFAs that promote autophagy and longevity (Lapierre et al., 2011; O'Rourke et al., 2013; O'Rourke and Ruvkun, 2013; Folick et al., 2015). Some of these FAs are escorted from the lysosome to the nucleus by the conserved lipid-binding protein LBP-8/FABP1 (Folick et al., 2015; Han and Brunet, 2015). In GSC(-) animals, SKN-1 nuclear accumulation was inhibited modestly by *lipl-4* RNAi but more strongly by *lipl-1/3* double knockdown (**Figure 6J**). Furthermore, *lipl-3* RNAi reduced stress resistance in GSC(-) but not WT animals (**Figure 6–figure supplements 3A and 3B**). Given that fat storage is increased in *lipl-1/3* mutants (O'Rourke and Ruvkun, 2013), our data suggest that in GSC(-) animals SKN-1 activity may depend upon particular *lipl-1/3*-dependent products, not lipid levels *per se*.

Knockdown of *lbp-8* or other LBPs also interfered with SKN-1::GFP nuclear accumulation in GSC(-) animals, and *lbp-8* RNAi impaired SKN-1-dependent *gst-4* activation by OA, indicating involvement of FA transport (**Figures 6J and 6K**). Together, our data suggest that in GSC(-) animals, excessive lipid levels lead to production of OA- and LIPL-1/3-dependent FAs that activate SKN-1, possibly through FA-based signaling (**Figure 7**).

Discussion

The question of how events in one tissue can influence aging in others is of fundamental importance. The effects of GSC loss in *C. elegans* provide a paradigm for investigating this problem, as well as interactions between a stem cell population and its environment. Here we determined that GSC inhibition leads to a broad transcriptional reprogramming in somatic tissues that involves activation of SKN-1, and that SKN-1 is required for many beneficial effects of GSC absence, including lifespan extension. Previous work showed that SKN-1 is required for lifespan to be extended by reduced insulin/IGF-1, mTORC1, or mTORC2 signaling, by dietary restriction, and by low-level mitochondrial ROS production (Bishop and Guarente, 2007; Tullet et al., 2008; Robida-Stubbs et al., 2012; Zarse et al., 2012; Schmeisser et al., 2013; Mizunuma et al., 2014; Moroz et al., 2014; Ewald et al., 2015). Our new data further support the idea that SKN-1/Nrf proteins are broadly important for longevity assurance.

One major role of SKN-1 in GSC(-) animals is to increase proteasome activity (**Figures 4C, 4D, and Figure 4–figure supplement 1**). In WT animals, SKN-1 activates most proteasome subunit genes when the proteasome is inhibited (Li et al., 2011). This compensatory function is conserved in its mammalian ortholog Nrf1, which

370 is cleaved and activated when proteasome activity is low (Radhakrishnan et al., 2010;
371 Steffen et al., 2010; Radhakrishnan et al., 2014; Sha and Goldberg, 2014). By contrast,
372 in GSC(-) animals proteasome activity is elevated (**Figures 4C, 4D**) (Vilchez et al.,
373 2012), suggesting that additional mechanisms influence SKN-1/Nrf regulation of
374 proteasome genes. In GSC(-) animals most if not all proteasome subunit genes are
375 dependent upon SKN-1 for their expression (**Figure 4A**), and SKN-1 and DAF-16
376 together activate the proteasome subunit gene *rpn-6.1* (**Figures 4E and 4F**), the levels
377 of which are rate-limiting for proteasome activity (Vilchez et al., 2012). Overexpression
378 of either *rpn-6.1* or the 20S proteasome subunit *pbs-5* increases *C. elegans* lifespan,
379 and in the latter case lifespan extension was shown to be *skn-1*-dependent (Vilchez et
380 al., 2012; Chondrogianni et al., 2015), suggesting that enhancement of proteasome
381 activity may be an important mechanism through which SKN-1/Nrf promotes longevity.
382 The evidence that GSC(-) longevity is associated with fat accumulation and
383 altered lipid metabolism has raised an intriguing possibility, that GSC absence induces
384 production of lipids that promote health and longevity (see **Introduction**). Our results
385 are consistent with aspects of this model, but suggest an important modification.
386 GSC(-) animals accumulate dramatically high levels of yolk lipoproteins by the first day
387 of adulthood (**Figures 6A and 6B**), providing a likely reason that they accumulate so
388 much lipid. Moreover, SKN-1 acts to *reduce* fat accumulation but is critical for the
389 benefits of GSC loss (**Figures 5B, 5C, and Figure 5–figure supplements 1A, 1B**),
390 suggesting that GSC(-) animals do not simply overproduce healthful lipids. Finally,
391 excess yolk accumulation induced by another method (*rme-2* RNAi) leads to increased
392 SKN-1 nuclear accumulation and target gene activation, and *skn-1*-dependent stress

393 resistance (**Figures 6D-6G**). Taken together, our data suggest that GSC(-) animals
394 accumulate excess fat because they cannot stop production of fat that would otherwise
395 support reproduction (**Figure 7**). Importantly, however, in responding to and
396 metabolizing this fat they produce specific lipids that activate SKN-1 and other
397 regulators, which in turn increase lifespan and may promote a more healthy balance of
398 lipids (**Figure 7**).
399 Several lines of evidence support this model. GSC inhibition induces SKN-1 and
400 NHR-49 to upregulate largely distinct sets of FA oxidation genes (**Figure 5A**)
401 (Ratnappan et al., 2014). This effect of SKN-1 could account for its inhibitory role in fat
402 accumulation (**Figures 5B and 5C**). A need to metabolize excess fat could also explain
403 the importance of lipophagy in GSC(-) longevity (Lapierre et al., 2011; Hansen et al.,
404 2013). With respect to signaling lipids, GSC(-) longevity requires the triglyceride lipase
405 LIPL-4 (Wang et al., 2008), which generates unsaturated FFAs that promote longevity
406 (O'Rourke et al., 2013; Folick et al., 2015). While LIPL-4-dependent FAs act through
407 NHR-49 and NHR-80 (Lapierre et al., 2011; Folick et al., 2015), and possibly not SKN-1
408 (**Figure 6J**), in GSC(-) animals SKN-1 activation involves the LIPL-1/3 lipases (**Figure**
409 **6J**), which also promote longevity (O'Rourke and Ruvkun, 2013). This elevated SKN-1
410 activity also depends upon lipid transfer proteins, as well as OA (**Figures 6H-6J and**
411 **Figure 6–figure supplement 1C**). OA is required for GSC(-) longevity (Goudeau et al.,
412 2011) and is a precursor to unsaturated FAs that have signaling functions (O'Rourke et
413 al., 2013; Folick et al., 2015). Finally, SKN-1 upregulates *lipl-3* and *lbp-8* in WT and
414 GSC(-) animals (**Figure 5A and Figure 5–figure supplement 3; Supplementary files**
415 **1a and 1c**), suggesting that it may function both downstream and upstream of lipid

signals. The idea that SKN-1 can be activated by lipids that arise from prevention of reproduction and yolk consumption should be considered in evaluation of genetic or pharmacological interventions that increase SKN-1 activity.

SKN-1 is activated by lipids and regulates lipid metabolism gene expression not only in the high-fat GSC(-) model, but also in WT animals under normal feeding conditions (**Figures 5 and 6; Supplementary files 1b-1d**). Moreover, SKN-1 profoundly reduced fat storage by the beginning of adult life in healthy, reproductively-active animals that have not begun to age. Taken together, our findings suggest that SKN-1 plays an integral and direct role in maintaining lipid homeostasis. Our results predict that insufficient mammalian Nrf function does not lead to NAFLD/NASH simply by increasing chronic hepatic stress (Xu et al., 2005; Lee et al., 2013), and that a protective function of Nrf proteins in fat metabolism is likely to be involved. Nrf proteins therefore may provide an important line of defense against metabolic disease. Development of NAFLD is a growing obesity-related public health issue (Cohen et al., 2011). Our data suggest that analysis of Nrf proteins could be a promising underexplored direction for investigating causes and prevention of NAFLD, and that SKN-1 and *C. elegans* provide a genetically tractable model that will be valuable in this effort.

Our evidence that GSCs activate SKN-1 through lipid-based signaling suggests a new mechanism through which GSCs influence the soma. The response to GSC loss therefore involves metabolic signals that reflect the altered nutritional balance within the organism. Similar interactions could be important in other stem cell contexts. For example, in the mammalian bone marrow microenvironment adipose tissue profoundly

influences the function of hematopoietic and mesenchymal stem cells (Adler et al., 2014; Muruganandan and Sinal, 2014). In addition to the mechanisms we have described, GSC(-) longevity involves endocrine signals from the somatic gonad and depends upon absence of GSCs *per se*, not simply reproductive cessation (Kenyon, 2010; Antebi, 2013). It will now be of interest to determine how these mechanisms, as well as other transcription factors that are required for GSC(-) longevity (see **Introduction**), interface with SKN-1 and its regulation.

Signaling lipids from endogenous, dietary or microbiota sources constitute an area of considerable excitement, because these signals can induce beneficial effects such as anti-inflammatory protection, enhanced insulin sensitivity, protection against metabolic disease, and increased lifespan in *C. elegans* (Wang et al., 2008; Kniazeva and Han, 2013; Lim et al., 2013; O'Rourke and Ruvkun, 2013; Folick et al., 2015; Han and Brunet, 2015). Signals derived from OA are of particular interest in this regard, because of its dietary availability in olive oil. Mechanisms through which lipid signals are known to act on transcription networks include binding to nuclear receptors, and OA-induced protein kinase A activation that ultimately leads to FA oxidation (Fu et al., 2003; Lim et al., 2013; Folick et al., 2015). By revealing SKN-1 as a new regulator of metabolism and stress defenses that is activated in response to lipids, our data suggest the exciting possibility that this might also be the case for mammalian Nrf proteins. They also suggest that a “lipohormesis” pathway in which signaling lipids confer health benefits by activating SKN-1/Nrf may not only be a characteristic of GSC-ablated animals, but also might be more broadly applicable for enhancing health- and possibly life-span.

Materials and methods

Strains

Worms were maintained on NGM plates seeded with *E. coli* (OP50) at 15°C, using standard techniques (Brenner, 1974). In all experiments, *glp-1(ts)* mutants were matched with the wild-type N2 strain used for outcrossing. The *C. elegans* strains used in this study are detailed in **Table 3**.

RNAi

Feeding RNAi was performed using tetracycline-resistant HT115 bacteria carrying the pL4440 plasmid with ampicillin/carbenicillin resistance (Kamath et al., 2001). RNAi cultures were grown overnight in 50 mL conical tubes at 37°C with shaking at 220 RPM in 5 mL LB medium containing 50 µg/mL carbenicillin and 12.5 µg/mL tetracycline. Cultures were diluted 1:5 the following day in LB containing carbenicillin and tetracycline to allow for re-entry into the logarithmic growth phase, grown to an OD_{600} of 1.5 (~6 hours). Cultures were centrifuged at 4,500 RPM for 10 minutes, concentrated to a volume of 5 mL, and then induced with 1 mM IPTG prior to plating. Bacterial cultures were seeded onto standard nematode growth medium (NGM) plates containing 50 µg/mL carbenicillin, 12.5 µg/mL tetracycline, and 0.4 mM IPTG.

Lifespans

Worms were synchronized by timed egg lay, upshifted to 25°C at the L2 stage, then scored for lifespan at 25°C or 20°C, as previously described (Arantes-Oliveira et al., 2002; Robida-Stubbs et al., 2012). For analyses of *glp-1(ts)* at 20°C, worms were downshifted from 25°C upon reaching adulthood. Animals were transferred at the first day of adulthood to fresh plates containing FUdR; ACROS Organics/Thermo Fisher

485 Scientific, Geel, Belgium) at a concentration of 100 µg/mL to inhibit progeny
486 development (Mitchell et al., 1979), unless otherwise indicated. RNAi-treated worms
487 were placed on RNAi feeding plates starting at the first day of adulthood. Worms were
488 maintained at a density of 30 worms per 6 cm plate on live bacteria, and scored every
489 other day. Animals that crawled off the plate, ruptured, or died from internal hatching
490 were censored. Lifespans were graphed as Kaplan-Meier survival curves with JMP Pro
491 12 (SAS Institute, Middleton, MA). *P* values for survival curve analysis were generated
492 using log-rank test. Additional statistical analysis was performed with GraphPad Prism
493 6 (GraphPad Software, La Jolla, CA). *P* values for mean lifespan analysis were
494 calculated by two-way ANOVA with post-hoc Holm-Šídák correction.

495 **Stress assays**

496 Synchronized animals were incubated at 25°C during development then scored
497 for survival hourly beginning at either days 1 or 3 of adulthood. Feeding RNAi was
498 started at the L1 stage for day 1 stress assays or post-developmentally at day 1
499 adulthood for stress assays performed at day 3 adulthood. For the arsenite stress
500 assay, worms were incubated in M9 buffer containing 5 mM sodium arsenite (Riedel-de
501 Haën, Seelze, Germany). For the tert-butyl hydroperoxide (TBHP) stress assay, worms
502 were placed on solid NGM plates containing 15.4 mM TBHP (Sigma-Aldrich, St. Louis,
503 MO). TBHP plates were freshly prepared on the day of the experiment. Survival
504 assays were graphed as Kaplan-Meier survival curves with JMP Pro 12. *P* values for
505 survival curve analysis were generated using log-rank test. Additional statistical
506 analysis was performed with GraphPad Prism 6. *P* values for mean survival analysis
507 were calculated by two-way ANOVA with post-hoc Holm-Šídák correction.

Microscopy

Animals were anaesthetized for 5 minutes in 0.06% tetramisole/M9 buffer, mounted on 2% agarose pads on glass slides under coverslips, and imaged with ZEN 2012 software on an Axio Imager.M2 microscope (Zeiss, Jena, Germany).

GFP reporter scoring

Intestinal SKN-1::GFP nuclear localization and *gst-4p*::GFP::NLS expression were scored as "high", "medium", or "low" as previously described (An and Blackwell, 2003; Ewald et al., 2015). "High" denotes strong intensity in all intestinal nuclei; "medium" indicates relatively lower intensity or distribution in approximately half of intestinal nuclei; "low" denotes weak or no visible GFP intensity in intestinal nuclei. *P* values were calculated by two-sided chi^2 test.

Intestinal DAF-16::GFP nuclear localization was scored as "high", "medium", or "low" as previously described (Henderson and Johnson, 2001; Berman and Kenyon, 2006; Curran and Ruvkun, 2007). "High" denotes more DAF-16::GFP observed in the nucleus compared to the cytoplasm; "medium" indicates animals with noticeable DAF-16::GFP in the nucleus but higher levels in the cytoplasm; "low" denotes entirely cytoplasmic DAF-16::GFP.

SKN-1::GFP color isolation was performed to reduce gut granule autofluorescence using selective color matching against rgb(99,159,94) with a fuzziness setting of 125 and auto contrast in Adobe Photoshop CC 2014 (Adobe, San Jose, CA). DAF-16::GFP color isolation was similarly performed using selective color matching against rgb(0,255,111) with a fuzziness setting of 100.

qRT-PCR

Samples were prepared from ~200 day 3 adult worms synchronized by timed egg lay. RNA was extracted using TRIzol (Thermo Fisher, Waltham, MA)-based phenol-chloroform extraction and purified with RNA Clean and Concentrator-5 spin columns (Zymo Research, Irvine, CA). RNA concentration and quality was assessed with a NanoDrop 1000 spectrophotometer (Thermo Fisher). cDNAs were prepared using SuperScript III First-Strand Synthesis SuperMix for qRT-PCR (Thermo Fisher). mRNA levels were quantified from biological triplicates and technical duplicates using SYBR Green (Thermo Fisher) fluorescence on a 384-well format Real Time PCR 7900 (Applied Biosystems, Foster City, CA). After an initial denaturation step (95°C for 10 min), amplification was performed using 40 cycles of denaturation (95°C for 15 s) and annealing (60°C for 1 min). Samples were analyzed by the standard curve method, with normalization to the reference genes *cdc-42* and Y45F10D.4 (Hoogewijs et al., 2008). *P* values were calculated by two-sided Student's t-test with post-hoc Holm-Šídák correction in GraphPad Prism 6. The primers were used in this study are provided in **Table 4**.

RNA sequencing (RNA-seq)

Samples were prepared from ~5,000 synchronized, L1 arrested day-one adult animals cultured at 25°C. Worms were synchronized by sodium hypochlorite (bleach) treatment, as previously described (Porta-de-la-Riva et al., 2012). Bleach solution (9 mL ddH2O; 1 mL 1 N NaOH; 4 mL Clorox bleach) was freshly prepared before each experiment. Worms were bleached for 5 minutes, washed 5x in M9, and arrested at the L1 stage at 25°C in M9 containing 10 µg/mL cholesterol. Feeding RNAi was started at

553 the L1 stage. This approach only partially reduces *skn-1* function, but allows analysis of
554 larger samples than would be feasible with *skn-1* mutants, which are sterile (Bowerman
555 et al., 1992). Because these animals were not treated with FUdR, the WT adults
556 contained an intact germline and eggs. As is explained in the **Results** section, we
557 therefore confined our analysis to genes that were overrepresented in *glp-1(ts)* animals,
558 which lack eggs and most of the germline, and established a high-confidence cutoff for
559 genes that were upregulated by GSC absence as opposed to simply being expressed
560 specifically in somatic tissues. RNA was extracted using the same protocol for qRT-
561 PCR samples. Purified RNA samples were DNase treated and assigned a RIN quality
562 score using a Bioanalyzer 2100 (Agilent Technologies, Santa Clara, CA). Only matched
563 samples with high RIN scores were sent for sequencing. Single read 50 bp RNA
564 sequencing with poly(A) enrichment was performed at the Dana-Farber Cancer Institute
565 Center for Computational Biology using a HiSeq 2000 (Illumina, San Diego, CA).
566 FASTQ output files were aligned to the WBcel235 (Feb 2014) *C. elegans*
567 reference genome using STAR (Dobin et al., 2013). These files have been deposited at
568 the Gene Expression Omnibus (GEO) with the accession number GSE63075. Samples
569 averaged 75% mapping of sequence reads to the reference genome. Differential
570 expression analysis was performed using a custom R and Bioconductor RNA-seq
571 pipeline (http://bioinf.wehi.edu.au/RNAseqCaseStudy/) (Gentleman et al., 2004; Anders
572 et al., 2013; R Core Team, 2014). Quantification of mapped reads in the aligned SAM
573 output files was performed using featureCounts, part of the Subread package (Liao et
574 al., 2013, 2014). We filtered out transcripts that didn't have at least one count per
575 million reads in at least two samples. Quantile normalization and estimation of the

mean-variance relationship of the log-counts was performed by voom (Law et al., 2014). Linear model fitting, empirical Bayes analysis and differential expression analysis was then conducted using limma (Smyth, 2005). To identify genes that are upregulated in a SKN-1-dependent manner by GSC loss, we sought genes for which *glp-1(ts)* expression was higher than WT, and for which *glp-1(ts);skn-1(-)* expression was reduced relative to *glp-1(ts)*. To test for this pattern, if a gene's expression change was higher in the comparison of *glp-1(ts)* vs. WT and lower in the comparison of *glp-1(ts);skn-1(-)* vs. *glp-1(ts),* then we calculated the minimum (in absolute value) of the *t*-statistics from these two comparisons, and assessed the significance of this statistic by comparing to a null distribution derived by applying this procedure to randomly generated *t*-statistics. We corrected for multiple testing in this and the differential expression analysis using the false discovery rate (FDR) (Benjamini and Hochberg, 1995). Heatmaps were generated using heatmap.2 in the gplots package (Warnes et al., 2014).

Functional annotations and phenotypes were obtained from Wormbase build WS246. SKN-1 transcription factor binding site analysis of hits was conducted with biomaRt, GenomicFeatures, JASPAR, MotifDb, motifStack, MotIV, and Rsamtools (Sandelin et al., 2004; Durinck et al., 2005; Durinck et al., 2009; Lawrence et al., 2013; Ou et al., 2013; Mercier and Gottardo, 2014; Shannon, 2014). JASPAR analysis was performed with the SKN-1 matrix MA0547.1 using 2 kb upstream sequences obtained from Ensembl WBcel235 (Staab et al., 2013). modENCODE SKN-1::GFP ChIP-seq analysis of hits was performed using biomaRt, ChIPpeakAnno, IRanges, and multtest (Durinck et al., 2005; Durinck et al., 2009; Gerstein et al., 2010; Zhu et al., 2010; Niu et al., 2011; Lawrence et al., 2013). SKN-1::GFP ChIP-seq peaks were generated by

599 Michael Snyder's lab. We used the peak data generated from the first 3 larval stages:
600 L1 (modENCODE_2622; GSE25810), L2 (modENCODE_3369), and L3
601 (modENCODE_3838; GSE48710). Human ortholog matching was performed using
602 Wormbase, Ensembl, and OrthoList (Shaye and Greenwald, 2011). Gene lists were
603 evaluated for functional classification and statistical overrepresentation with Database
604 for Annotation, Visualization and Integrated Discovery (DAVID) version 6.7 (Dennis et
605 al., 2003).

606 ***rpn-6.1* binding site analysis**

607 SKN-1 and DAF-16 binding peaks within the first intron and the promoter of *rpn-*
608 *6.1* were previously identified by the modENCODE project (Furuyama et al., 2000;
609 Gerstein et al., 2010; Niu et al., 2011). We identified multiple hits with the consensus
610 binding sequence ATCAT in the TRANSFAC matrices N$SKN1_01 and N$SKN1_02
611 using MATCH (BioBase) that overlap with the SKN-1::GFP ChIP-seq binding peaks
612 within the first intron and the promoter of *rpn-6.1* (Kel et al., 2003; Matys et al., 2006).
613 Our analysis also confirmed a previously identified hit (Vilchez et al., 2012) in the
614 N$DAF16_01 matrix with the consensus binding sequence TGTTT that overlaps with
615 the DAF-16::GFP ChIP-seq peak within the first intron. No putative DAF-16 binding
616 sites were identified in the *rpn-6.1* promoter in the TRANSFAC MATCH analysis.

617 **Proteasome activity**

618 In vitro chymotrypsin-like proteasome activity assays were performed as
619 previously described (Kisselev and Goldberg, 2005; Vilchez et al., 2012). Worms were
620 bleach synchronized and maintained at 25°C from egg stage, then lysed at day 1 of
621 adulthood, unless otherwise noted, in freshly prepared proteasome activity assay buffer

(50 mM Tris-HCl, pH 7, 250 mM sucrose, 5 mM $MgCl_2$, 0.5 mM EDTA, 2 mM ATP and 1 mM dithiothreitol) using a Branson digital sonifier at 4°C. Lysates were centrifuged at 10,000 x g for 15 min at 4°C. 25 µg of protein, calculated using the BCA protein assay (#23225; Pierce Biotechnology/Thermo Fisher, Rockford, IL), was transferred to a flat 96-well microtiter plate (Nunc, Roskilde, Denmark). Samples were incubated at 25°C and fluorogenic chymotrypsin substrate (#230914; Calbiochem/EMD Millipore, San Diego, CA) was added to the plate immediately before analysis. Fluorescence (380 nm excitation; 460 nm emission) was measured every 3 min for 1 h at 25°C using a Synergy MX microplate reader with Gen5 software (Bio-Tek, Winooski, VT). Lysates were assayed in triplicate. *P* values were calculated by two-sided Student's *t*-test in GraphPad Prism 6.

Fixed oil red O (ORO) staining

ORO staining was performed on fixed animals, essentially as described (O'Rourke et al., 2009; Yen et al., 2010), with some modifications. 200-300 day-one adult worms synchronized by timed egg lay were washed three times with PBS then snap frozen in a dry ice/ethanol bath. Upon thawing, worms were treated with PBS containing 2% paraformaldehyde (PFA), using 3 freeze thaw cycles with dry ice/ethanol to permeabilize the cuticle. Worms were then washed with PBS to remove the PFA. Filtered ORO solution (0.5 g of ORO powder [#O0625; Sigma-Aldrich] in 100 mL of 60% isopropanol) was prepared freshly before each experiment. Worms were stained for 3 hours in a round bottom 96 well plate in ORO solution at room temperature with gentle shaking. Longer staining periods, such as overnight incubation (O'Rourke et al., 2009),

saturated ORO staining in *glp-1(ts)* animals to a level that rendered *glp-1(ts)* and *glp-1(ts);skn-1* strains indistinguishable.

Animals were imaged at 40X using differential interference contrast (DIC) microscopy. Quantification of ORO staining was performed on the upper intestine, directly below the pharynx. Since ORO absorbs light at 510 nm (green channel), we performed background subtraction of the red channel from the green channel in Adobe Photoshop CC (Adobe, San Jose, CA) to specifically isolate the ORO staining, as previously described (Yen et al., 2010). Quantification of mean intensity over background for each animal was performed using Fiji (http://fiji.sc). Statistical analysis was performed with GraphPad Prism 6. *P* values were calculated by one-way ANOVA with post-hoc Holm-Šídák correction.

DHS-3::GFP scoring

Using a COPAS Biosort (Union Biometrica, Holliston, MA) (Pulak, 2006), bleach-synchronized day-one adult worms were scored for GFP fluorescence. RNAi was initiated after L1 arrest. The COPAS was used to record three attributes for each individual nematode: time of flight (TOF), which corresponds to nematode length; extinction (EXT), which corresponds to the optical density; and GFP fluorescence intensity. TOF and EXT measurements are related to the size and age of the nematode; both increase with development. These parameters were used to specifically gate adult worms. GFP fluorescence was normalized to worm size as a ratio of GFP/TOF values. Representative GFP images of each strain were captured at 4X using an Olympus IX51 inverted microscope (Olympus, New Orleans, LA). *P* values

were calculated by one-way ANOVA with post-hoc Holm-Šídák correction in GraphPad Prism 6.

Triglyceride quantification

Triglyceride (TAG) levels were measured with the Triglyceride Colorimetric Assay Kit (#10010303; Cayman Chemical, Ann Arbor, MI). Samples were run according to the manufacturer's protocol in triplicate. TAG concentrations were normalized relative to protein concentration using the BCA protein assay (Pierce Biotechnology).

Acknowledgements

We thank Adam Antebi, Cynthia Kenyon, and Pingsheng Liu for strains, Javier Apfeld, William Mair, and Blackwell lab members for helpful discussions, and Sneha Rath and Collin Ewald for contributions to early stages of this work. Some strains were provided by the *Caenorhabditis* Genetics Center (CGC), which is funded by NIH Office of Research Infrastructure Programs (P40 OD010440).

Competing interests

The authors declare that no competing interests exist. The funders had no role in study design, data collection and interpretation, or the decision to submit the work for publication.

References

Ackerman, D., and Gems, D. (2012). The mystery of C. elegans aging: an emerging role for fat. Distant parallels between C. elegans aging and metabolic syndrome? Bioessays 34:466-71. doi:10.1002/bies.201100189

Adler, B.J., Kaushansky, K., and Rubin, C.T. (2014). Obesity-driven disruption of haematopoiesis and the bone marrow niche. Nat Rev Endocrinol 10:737-48. doi:10.1038/nrendo.2014.169

Alper, S., McElwee, M.K., Apfeld, J., Lackford, B., Freedman, J.H., and Schwartz, D.A. (2010). The Caenorhabditis elegans germ line regulates distinct signaling pathways to control lifespan and innate immunity. J Biol Chem 285:1822-8. doi:10.1074/jbc.M109.057323

An, J.H., and Blackwell, T.K. (2003). SKN-1 links C. elegans mesendodermal specification to a conserved oxidative stress response. Genes Dev 17:1882-93. doi:10.1101/gad.1107803

Anders, S., McCarthy, D.J., Chen, Y., Okoniewski, M., Smyth, G.K., Huber, W., and Robinson, M.D. (2013). Count-based differential expression analysis of RNA sequencing data using R and Bioconductor. Nat Protoc 8:1765-86. doi:10.1038/nprot.2013.099

Antebi, A. (2013). Regulation of longevity by the reproductive system. Exp Gerontol 48:596-602. doi:10.1016/j.exger.2012.09.009

Arantes-Oliveira, N., Apfeld, J., Dillin, A., and Kenyon, C. (2002). Regulation of life-span by germ-line stem cells in Caenorhabditis elegans. Science 295:502-5. doi:10.1126/science.1065768

Ben-Zvi, A., Miller, E.A., and Morimoto, R.I. (2009). Collapse of proteostasis represents an early molecular event in Caenorhabditis elegans aging. Proc Natl Acad Sci U S A 106:14914-9. doi:10.1073/pnas.0902882106

Benjamini, Y., and Hochberg, Y. (1995). Controlling the False Discovery Rate: A Practical and Powerful Approach to Multiple Testing. Journal of the Royal Statistical Society. Series B (Methodological) 57:289-300. doi:10.2307/2346101

Berman, J.R., and Kenyon, C. (2006). Germ-cell loss extends C. elegans life span through regulation of DAF-16 by kri-1 and lipophilic-hormone signaling. Cell 124:1055-68. doi:10.1016/j.cell.2006.01.039

Bishop, N.A., and Guarente, L. (2007). Two neurons mediate diet-restriction-induced longevity in C. elegans. Nature 447:545-9. doi:10.1038/nature05904

717 Bowerman, B., Eaton, B.A., and Priess, J.R. (1992). skn-1, a maternally expressed
718 gene required to specify the fate of ventral blastomeres in the early C. elegans embryo.
719 Cell 68:1061-75.

720 Brenner, S. (1974). The genetics of Caenorhabditis elegans. Genetics 77:71-94.

721 Chikina, M.D., Huttenhower, C., Murphy, C.T., and Troyanskaya, O.G. (2009). Global
722 prediction of tissue-specific gene expression and context-dependent gene networks in
723 Caenorhabditis elegans. PLoS Comput Biol 5:e1000417.
724 doi:10.1371/journal.pcbi.1000417

725 Choe, K.P., Przybysz, A.J., and Strange, K. (2009). The WD40 repeat protein WDR-23
726 functions with the CUL4/DDB1 ubiquitin ligase to regulate nuclear abundance and
727 activity of SKN-1 in Caenorhabditis elegans. Mol Cell Biol 29:2704-15.
728 doi:10.1128/MCB.01811-08

729 Chondrogianni, N., Georgila, K., Kourtis, N., Tavernarakis, N., and Gonos, E.S. (2015).
730 20S proteasome activation promotes life span extension and resistance to proteotoxicity
731 in Caenorhabditis elegans. FASEB J 29:611-22. doi:10.1096/fj.14-252189

732 Cohen, J.C., Horton, J.D., and Hobbs, H.H. (2011). Human fatty liver disease: old
733 questions and new insights. Science 332:1519-23. doi:10.1126/science.1204265

734 Curran, S.P., and Ruvkun, G. (2007). Lifespan regulation by evolutionarily conserved
735 genes essential for viability. PLoS Genet 3:e56. doi:10.1371/journal.pgen.0030056

736 Dennis, G., Jr., Sherman, B.T., Hosack, D.A., Yang, J., Gao, W., Lane, H.C., and
737 Lempicki, R.A. (2003). DAVID: Database for Annotation, Visualization, and Integrated
738 Discovery. Genome Biol 4:P3.

739 Dobin, A., Davis, C.A., Schlesinger, F., Drenkow, J., Zaleski, C., Jha, S., Batut, P.,
740 Chaisson, M., and Gingeras, T.R. (2013). STAR: ultrafast universal RNA-seq aligner.
741 Bioinformatics 29:15-21. doi:10.1093/bioinformatics/bts635

742 Dorsett, M., Westlund, B., and Schedl, T. (2009). METT-10, a putative
743 methyltransferase, inhibits germ cell proliferative fate in Caenorhabditis elegans.
744 Genetics 183:233-47. doi:10.1534/genetics.109.105270

745 Durinck, S., Moreau, Y., Kasprzyk, A., Davis, S., De Moor, B., Brazma, A., and Huber,
746 W. (2005). BioMart and Bioconductor: a powerful link between biological databases and
747 microarray data analysis. Bioinformatics 21:3439-40. doi:10.1093/bioinformatics/bti525

748 Durinck, S., Spellman, P.T., Birney, E., and Huber, W. (2009). Mapping identifiers for
749 the integration of genomic datasets with the R/Bioconductor package biomaRt. Nat
750 Protoc 4:1184-91. doi:10.1038/nprot.2009.97

751 Ewald, C.Y., Landis, J.N., Abate, J.P., Murphy, C.T., and Blackwell, T.K. (2015). Dauer-
752 independent insulin/IGF-1-signalling implicates collagen remodelling in longevity. Nature
753 519:97-101. doi:10.1038/nature14021

754 Flatt, T., Min, K.J., D'Alterio, C., Villa-Cuesta, E., Cumbers, J., Lehmann, R., Jones,
755 D.L., and Tatar, M. (2008). Drosophila germ-line modulation of insulin signaling and
756 lifespan. Proc Natl Acad Sci U S A 105:6368-73. doi:10.1073/pnas.0709128105

757 Folick, A., Oakley, H.D., Yu, Y., Armstrong, E.H., Kumari, M., Sanor, L., Moore, D.D.,
758 Ortlund, E.A., Zechner, R., and Wang, M.C. (2015). Aging. Lysosomal signaling
759 molecules regulate longevity in Caenorhabditis elegans. Science 347:83-6.
760 doi:10.1126/science.1258857

761 Fu, J., Gaetani, S., Oveisi, F., Lo Verme, J., Serrano, A., Rodriguez De Fonseca, F.,
762 Rosengarth, A., Luecke, H., Di Giacomo, B., Tarzia, G., et al. (2003). Oleylethanolamide
763 regulates feeding and body weight through activation of the nuclear receptor PPAR-
764 alpha. Nature 425:90-3. doi:10.1038/nature01921

765 Furuyama, T., Nakazawa, T., Nakano, I., and Mori, N. (2000). Identification of the
766 differential distribution patterns of mRNAs and consensus binding sequences for mouse
767 DAF-16 homologues. Biochem J 349:629-34.

768 Gentleman, R.C., Carey, V.J., Bates, D.M., Bolstad, B., Dettling, M., Dudoit, S., Ellis, B.,
769 Gautier, L., Ge, Y., Gentry, J., et al. (2004). Bioconductor: open software development
770 for computational biology and bioinformatics. Genome Biol 5:R80. doi:10.1186/gb-2004-
771 5-10-r80

772 Gerstein, M.B., Lu, Z.J., Van Nostrand, E.L., Cheng, C., Arshinoff, B.I., Liu, T., Yip, K.Y.,
773 Robilotto, R., Rechtsteiner, A., Ikegami, K., et al. (2010). Integrative analysis of the
774 Caenorhabditis elegans genome by the modENCODE project. Science 330:1775-87.
775 doi:10.1126/science.1196914

776 Ghazi, A., Henis-Korenblit, S., and Kenyon, C. (2009). A transcription elongation factor
777 that links signals from the reproductive system to lifespan extension in Caenorhabditis
778 elegans. PLoS Genet 5:e1000639. doi:10.1371/journal.pgen.1000639

779 Glickman, M.H., and Ciechanover, A. (2002). The ubiquitin-proteasome proteolytic
780 pathway: destruction for the sake of construction. Physiol Rev 82:373-428.
781 doi:10.1152/physrev.00027.2001

782 Goldberg, A.L. (2003). Protein degradation and protection against misfolded or
783 damaged proteins. Nature 426:895-9. doi:10.1038/nature02263

784 Goudeau, J., Bellemin, S., Toselli-Mollereau, E., Shamalnasab, M., Chen, Y., and
785 Aguilaniu, H. (2011). Fatty acid desaturation links germ cell loss to longevity through
786 NHR-80/HNF4 in C. elegans. PLoS Biol 9:e1000599. doi:10.1371/journal.pbio.1000599

787 Grant, B., and Hirsh, D. (1999). Receptor-mediated endocytosis in the Caenorhabditis
788 elegans oocyte. Mol Biol Cell 10:4311-26.

789 Han, S., and Brunet, A. (2015). Cell biology. Lysosomal lipid lengthens life span.
790 Science 347:32-3. doi:10.1126/science.aaa4565

791 Hansen, M., Flatt, T., and Aguilaniu, H. (2013). Reproduction, fat metabolism, and life
792 span: what is the connection? Cell Metab 17:10-9. doi:10.1016/j.cmet.2012.12.003

793 Hayes, J.D., and Dinkova-Kostova, A.T. (2014). The Nrf2 regulatory network provides
794 an interface between redox and intermediary metabolism. Trends Biochem Sci 39:199-
795 218. doi:10.1016/j.tibs.2014.02.002

796 Henderson, S.T., and Johnson, T.E. (2001). daf-16 integrates developmental and
797 environmental inputs to mediate aging in the nematode Caenorhabditis elegans. Curr
798 Biol 11:1975-80.

799 Hoogewijs, D., Houthoofd, K., Matthijssens, F., Vandesompele, J., and Vanfleteren, J.R.
800 (2008). Selection and validation of a set of reliable reference genes for quantitative sod
801 gene expression analysis in C. elegans. BMC Mol Biol 9:9. doi:10.1186/1471-2199-9-9

802 Hsin, H., and Kenyon, C. (1999). Signals from the reproductive system regulate the
803 lifespan of C. elegans. Nature 399:362-6. doi:10.1038/20694

804 Inoue, H., Hisamoto, N., An, J.H., Oliveira, R.P., Nishida, E., Blackwell, T.K., and
805 Matsumoto, K. (2005). The C. elegans p38 MAPK pathway regulates nuclear
806 localization of the transcription factor SKN-1 in oxidative stress response. Genes Dev
807 19:2278-83. doi:10.1101/gad.1324805

808 Jones, D.L., and Wagers, A.J. (2008). No place like home: anatomy and function of the
809 stem cell niche. Nat Rev Mol Cell Biol 9:11-21. doi:10.1038/nrm2319

810 Kamath, R.S., Martinez-Campos, M., Zipperlen, P., Fraser, A.G., and Ahringer, J.
811 (2001). Effectiveness of specific RNA-mediated interference through ingested double-
812 stranded RNA in Caenorhabditis elegans. Genome Biol 2:RESEARCH0002.
813 doi:10.1186/gb-2000-2-1-research0002

814 Kel, A.E., Gossling, E., Reuter, I., Cheremushkin, E., Kel-Margoulis, O.V., and
815 Wingender, E. (2003). MATCH: A tool for searching transcription factor binding sites in
816 DNA sequences. Nucleic Acids Res 31:3576-9.

817 Kenyon, C.J. (2010). The genetics of ageing. Nature 464:504-12.
818 doi:10.1038/nature08980

819 Kimble, J., and Crittenden, S.L. (2005). Germline proliferation and its control.
820 WormBook1-14. doi:10.1895/wormbook.1.13.1

821 Kisselev, A.F., and Goldberg, A.L. (2005). Monitoring activity and inhibition of 26S
822 proteasomes with fluorogenic peptide substrates. Methods Enzymol 398:364-78.
823 doi:10.1016/S0076-6879(05)98030-0

824 Kniazeva, M., and Han, M. (2013). Fat chance for longevity. Genes Dev 27:351-4.
825 doi:10.1101/gad.214189.113

826 Kokatnur, M.G., Oalmann, M.C., Johnson, W.D., Malcom, G.T., and Strong, J.P. (1979).
827 Fatty acid composition of human adipose tissue from two anatomical sites in a biracial
828 community. Am J Clin Nutr 32:2198-205.

829 Lapierre, L.R., Gelino, S., Melendez, A., and Hansen, M. (2011). Autophagy and lipid
830 metabolism coordinately modulate life span in germline-less C. elegans. Curr Biol
831 21:1507-14. doi:10.1016/j.cub.2011.07.042

832 Law, C.W., Chen, Y., Shi, W., and Smyth, G.K. (2014). voom: precision weights unlock
833 linear model analysis tools for RNA-seq read counts. Genome Biol 15:R29.
834 doi:10.1186/gb-2014-15-2-r29

835 Lawrence, M., Huber, W., Pages, H., Aboyoun, P., Carlson, M., Gentleman, R., Morgan,
836 M.T., and Carey, V.J. (2013). Software for computing and annotating genomic ranges.
837 PLoS Comput Biol 9:e1003118. doi:10.1371/journal.pcbi.1003118

838 Lee, C.S., Ho, D.V., and Chan, J.Y. (2013). Nuclear factor-erythroid 2-related factor 1
839 regulates expression of proteasome genes in hepatocytes and protects against
840 endoplasmic reticulum stress and steatosis in mice. FEBS J 280:3609-20.
841 doi:10.1111/febs.12350

842 Leiser, S.F., and Miller, R.A. (2010). Nrf2 signaling, a mechanism for cellular stress
843 resistance in long-lived mice. Mol Cell Biol 30:871-84. doi:10.1128/MCB.01145-09

844 Li, X., Matilainen, O., Jin, C., Glover-Cutter, K.M., Holmberg, C.I., and Blackwell, T.K.
845 (2011). Specific SKN-1/Nrf stress responses to perturbations in translation elongation
846 and proteasome activity. PLoS Genet 7:e1002119. doi:10.1371/journal.pgen.1002119

847 Liao, Y., Smyth, G.K., and Shi, W. (2013). The Subread aligner: fast, accurate and
848 scalable read mapping by seed-and-vote. Nucleic Acids Res 41:e108.
849 doi:10.1093/nar/gkt214

850 Liao, Y., Smyth, G.K., and Shi, W. (2014). featureCounts: an efficient general purpose
851 program for assigning sequence reads to genomic features. Bioinformatics 30:923-30.
852 doi:10.1093/bioinformatics/btt656

853 Libina, N., Berman, J.R., and Kenyon, C. (2003). Tissue-specific activities of C. elegans
854 DAF-16 in the regulation of lifespan. Cell 115:489-502.

855 Lim, J.H., Gerhart-Hines, Z., Dominy, J.E., Lee, Y., Kim, S., Tabata, M., Xiang, Y.K.,
856 and Puigserver, P. (2013). Oleic acid stimulates complete oxidation of fatty acids

through protein kinase A-dependent activation of SIRT1-PGC1alpha complex. J Biol Chem 288:7117-26. doi:10.1074/jbc.M112.415729

Lin, K., Hsin, H., Libina, N., and Kenyon, C. (2001). Regulation of the Caenorhabditis elegans longevity protein DAF-16 by insulin/IGF-1 and germline signaling. Nat Genet 28:139-45. doi:10.1038/88850

Link, C.D., and Johnson, C.J. (2002). Reporter transgenes for study of oxidant stress in Caenorhabditis elegans. Methods Enzymol 353:497-505.

Matys, V., Kel-Margoulis, O.V., Fricke, E., Liebich, I., Land, S., Barre-Dirrie, A., Reuter, I., Chekmenev, D., Krull, M., Hornischer, K., et al. (2006). TRANSFAC and its module TRANSCompel: transcriptional gene regulation in eukaryotes. Nucleic Acids Res 34:D108-10. doi:10.1093/nar/gkj143

McCormick, M., Chen, K., Ramaswamy, P., and Kenyon, C. (2012). New genes that extend Caenorhabditis elegans' lifespan in response to reproductive signals. Aging Cell 11:192-202. doi:10.1111/j.1474-9726.2011.00768.x

Mercier, E., and Gottardo, R. (2014). MotIV: Motif Identification and Validation.

Min, K.J., Lee, C.K., and Park, H.N. (2012). The lifespan of Korean eunuchs. Curr Biol 22:R792-3. doi:10.1016/j.cub.2012.06.036

Mitchell, D.H., Stiles, J.W., Santelli, J., and Sanadi, D.R. (1979). Synchronous growth and aging of Caenorhabditis elegans in the presence of fluorodeoxyuridine. J Gerontol 34:28-36.

Mizunuma, M., Neumann-Haefelin, E., Moroz, N., Li, Y., and Blackwell, T.K. (2014). mTORC2-SGK-1 acts in two environmentally responsive pathways with opposing effects on longevity. Aging Cell 13:869-78. doi:10.1111/acel.12248

Moerman, D.G., and Williams, B.D. (2006). Sarcomere assembly in C. elegans muscle. WormBook1-16. doi:10.1895/wormbook.1.81.1

Moroz, N., Carmona, J.J., Anderson, E., Hart, A.C., Sinclair, D.A., and Blackwell, T.K. (2014). Dietary restriction involves NAD(+) -dependent mechanisms and a shift toward oxidative metabolism. Aging Cell 13:1075-85. doi:10.1111/acel.12273

Murphy, C.T., McCarroll, S.A., Bargmann, C.I., Fraser, A., Kamath, R.S., Ahringer, J., Li, H., and Kenyon, C. (2003). Genes that act downstream of DAF-16 to influence the lifespan of Caenorhabditis elegans. Nature 424:277-83. doi:10.1038/nature01789

Muruganandan, S., and Sinal, C.J. (2014). The impact of bone marrow adipocytes on osteoblast and osteoclast differentiation. IUBMB Life 66:147-55. doi:10.1002/iub.1254

Na, H., Zhang, P., Chen, Y., Zhu, X., Liu, Y., Liu, Y., Xie, K., Xu, N., Yang, F., Yu, Y., et al. (2015). Identification of Lipid Droplet Structure-like/Resident Proteins in

892 Caenorhabditis elegans. Biochimica et Biophysica Acta (BBA) - Molecular Cell
893 Research. doi:10.1016/j.bbamcr.2015.05.020

894 National Research Council (1976). Fat Content and Composition of Animal Products.
895 (Washington, DC: Printing and Publishing Office, National Academy of Sciences).

896 Niu, W., Lu, Z.J., Zhong, M., Sarov, M., Murray, J.I., Brdlik, C.M., Janette, J., Chen, C.,
897 Alves, P., Preston, E., et al. (2011). Diverse transcription factor binding features
898 revealed by genome-wide ChIP-seq in C. elegans. Genome Res 21:245-54.
899 doi:10.1101/gr.114587.110

900 O'Rourke, E.J., Kuballa, P., Xavier, R., and Ruvkun, G. (2013). omega-6
901 Polyunsaturated fatty acids extend life span through the activation of autophagy. Genes
902 Dev 27:429-40. doi:10.1101/gad.205294.112

903 O'Rourke, E.J., and Ruvkun, G. (2013). MXL-3 and HLH-30 transcriptionally link
904 lipolysis and autophagy to nutrient availability. Nat Cell Biol 15:668-76.
905 doi:10.1038/ncb2741

906 O'Rourke, E.J., Soukas, A.A., Carr, C.E., and Ruvkun, G. (2009). C. elegans major fats
907 are stored in vesicles distinct from lysosome-related organelles. Cell Metab 10:430-5.
908 doi:10.1016/j.cmet.2009.10.002

909 Okada, K., Warabi, E., Sugimoto, H., Horie, M., Gotoh, N., Tokushige, K., Hashimoto,
910 E., Utsunomiya, H., Takahashi, H., Ishii, T., et al. (2013). Deletion of Nrf2 leads to rapid
911 progression of steatohepatitis in mice fed atherogenic plus high-fat diet. J Gastroenterol
912 48:620-32. doi:10.1007/s00535-012-0659-z

913 Oliveira, R.P., Porter Abate, J., Dilks, K., Landis, J., Ashraf, J., Murphy, C.T., and
914 Blackwell, T.K. (2009). Condition-adapted stress and longevity gene regulation by
915 Caenorhabditis elegans SKN-1/Nrf. Aging Cell 8:524-41. doi:10.1111/j.1474-
916 9726.2009.00501.x

917 Ou, J., Brodsky, M., Wolfe, S., and Zhu, L.J. (2013). motifStack: Plot stacked logos for
918 single or multiple DNA, RNA and amino acid sequence.

919 Paek, J., Lo, J.Y., Narasimhan, S.D., Nguyen, T.N., Glover-Cutter, K., Robida-Stubbs,
920 S., Suzuki, T., Yamamoto, M., Blackwell, T.K., and Curran, S.P. (2012). Mitochondrial
921 SKN-1/Nrf mediates a conserved starvation response. Cell Metab 16:526-37.
922 doi:10.1016/j.cmet.2012.09.007

923 Pang, S., Lynn, D.A., Lo, J.Y., Paek, J., and Curran, S.P. (2014). SKN-1 and Nrf2
924 couples proline catabolism with lipid metabolism during nutrient deprivation. Nat
925 Commun 5:5048. doi:10.1038/ncomms6048

926 Park, S.K., Tedesco, P.M., and Johnson, T.E. (2009). Oxidative stress and longevity in
927 Caenorhabditis elegans as mediated by SKN-1. Aging Cell 8:258-69.
928 doi:10.1111/j.1474-9726.2009.00473.x

929 Partridge, L., Gems, D., and Withers, D.J. (2005). Sex and death: what is the
930 connection? Cell 120:461-72. doi:10.1016/j.cell.2005.01.026

931 Porta-de-la-Riva, M., Fontrodona, L., Villanueva, A., and Ceron, J. (2012). Basic
932 Caenorhabditis elegans methods: synchronization and observation. J Vis Expe4019.
933 doi:10.3791/4019

934 Pulak, R. (2006). Techniques for analysis, sorting, and dispensing of C. elegans on the
935 COPAS flow-sorting system. Methods Mol Biol 351:275-86. doi:10.1385/1-59745-151-
936 7:275

937 R Core Team (2014). R: A Language and Environment for Statistical Computing.
938 (Vienna, Austria). http://www.R-project.org/

939 Radhakrishnan, S.K., den Besten, W., and Deshaies, R.J. (2014). p97-dependent
940 retrotranslocation and proteolytic processing govern formation of active Nrf1 upon
941 proteasome inhibition. Elife 3:e01856. doi:10.7554/eLife.01856

942 Radhakrishnan, S.K., Lee, C.S., Young, P., Beskow, A., Chan, J.Y., and Deshaies, R.J.
943 (2010). Transcription factor Nrf1 mediates the proteasome recovery pathway after
944 proteasome inhibition in mammalian cells. Mol Cell 38:17-28.
945 doi:10.1016/j.molcel.2010.02.029

946 Ratnappan, R., Amrit, F.R., Chen, S.W., Gill, H., Holden, K., Ward, J., Yamamoto, K.R.,
947 Olsen, C.P., and Ghazi, A. (2014). Germline Signals Deploy NHR-49 to Modulate Fatty-
948 Acid beta-Oxidation and Desaturation in Somatic Tissues of C. elegans. PLoS Genet
949 10:e1004829. doi:10.1371/journal.pgen.1004829

950 Richmond, J. (2005). Synaptic function. WormBook1-14. doi:10.1895/wormbook.1.69.1

951 Robida-Stubbs, S., Glover-Cutter, K., Lamming, D.W., Mizunuma, M., Narasimhan,
952 S.D., Neumann-Haefelin, E., Sabatini, D.M., and Blackwell, T.K. (2012). TOR signaling
953 and rapamycin influence longevity by regulating SKN-1/Nrf and DAF-16/FoxO. Cell
954 Metab 15:713-24. doi:10.1016/j.cmet.2012.04.007

955 Sandelin, A., Alkema, W., Engstrom, P., Wasserman, W.W., and Lenhard, B. (2004).
956 JASPAR: an open-access database for eukaryotic transcription factor binding profiles.
957 Nucleic Acids Res 32:D91-4. doi:10.1093/nar/gkh012

958 Schmeisser, S., Schmeisser, K., Weimer, S., Groth, M., Priebe, S., Fazius, E., Kuhlow,
959 D., Pick, D., Einax, J.W., Guthke, R., et al. (2013). Mitochondrial hormesis links low-
960 dose arsenite exposure to lifespan extension. Aging Cell 12:508-17.
961 doi:10.1111/acel.12076

962 Sha, Z., and Goldberg, A.L. (2014). Proteasome-mediated processing of Nrf1 is
963 essential for coordinate induction of all proteasome subunits and p97. Curr Biol
964 24:1573-83. doi:10.1016/j.cub.2014.06.004

965 Shannon, P. (2014). MotifDb: An Annotated Collection of Protein-DNA Binding
966 Sequence Motifs.

967 Shaye, D.D., and Greenwald, I. (2011). OrthoList: a compendium of C. elegans genes
968 with human orthologs. PLoS One 6:e20085. doi:10.1371/journal.pone.0020085

969 Shen, Y., Wollam, J., Magner, D., Karalay, O., and Antebi, A. (2012). A steroid receptor-
970 microRNA switch regulates life span in response to signals from the gonad. Science
971 338:1472-6. doi:10.1126/science.1228967

972 Smyth, G.K. (2005). limma: Linear Models for Microarray Data. 397-420. doi:10.1007/0-
973 387-29362-0_23

974 Staab, T.A., Griffen, T.C., Corcoran, C., Evgrafov, O., Knowles, J.A., and Sieburth, D.
975 (2013). The conserved SKN-1/Nrf2 stress response pathway regulates synaptic function
976 in Caenorhabditis elegans. PLoS Genet 9:e1003354. doi:10.1371/journal.pgen.1003354

977 Steffen, J., Seeger, M., Koch, A., and Kruger, E. (2010). Proteasomal degradation is
978 transcriptionally controlled by TCF11 via an ERAD-dependent feedback loop. Mol Cell
979 40:147-58. doi:10.1016/j.molcel.2010.09.012

980 Steinbaugh, M.J., Sun, L.Y., Bartke, A., and Miller, R.A. (2012). Activation of genes
981 involved in xenobiotic metabolism is a shared signature of mouse models with extended
982 lifespan. Am J Physiol Endocrinol Metab 303:E488-95.
983 doi:10.1152/ajpendo.00110.2012

984 Sykiotis, G.P., and Bohmann, D. (2010). Stress-activated cap'n'collar transcription
985 factors in aging and human disease. Sci Signal 3:re3. doi:10.1126/scisignal.3112re3

986 Tsujita, T., Peirce, V., Baird, L., Matsuyama, Y., Takaku, M., Walsh, S.V., Griffin, J.L.,
987 Uruno, A., Yamamoto, M., and Hayes, J.D. (2014). Transcription factor Nrf1 negatively
988 regulates the cystine/glutamate transporter and lipid-metabolizing enzymes. Mol Cell
989 Biol 34:3800-16. doi:10.1128/MCB.00110-14

990 Tullet, J.M., Hertweck, M., An, J.H., Baker, J., Hwang, J.Y., Liu, S., Oliveira, R.P.,
991 Baumeister, R., and Blackwell, T.K. (2008). Direct inhibition of the longevity-promoting
992 factor SKN-1 by insulin-like signaling in C. elegans. Cell 132:1025-38.
993 doi:10.1016/j.cell.2008.01.030

994 Vilchez, D., Morantte, I., Liu, Z., Douglas, P.M., Merkwirth, C., Rodrigues, A.P.,
995 Manning, G., and Dillin, A. (2012). RPN-6 determines C. elegans longevity under
996 proteotoxic stress conditions. Nature 489:263-8. doi:10.1038/nature11315

997 Wang, M.C., O'Rourke, E.J., and Ruvkun, G. (2008). Fat metabolism links germline
998 stem cells and longevity in C. elegans. Science 322:957-60.
999 doi:10.1126/science.1162011

1000 Warnes, G.R., Bolker, B., Bonebakker, L., Gentleman, R., Liaw, W.H.A., Lumley, T.,
1001 Maechler, M., Magnusson, A., Moeller, S., Schwartz, M., et al. (2014). gplots: Various R
1002 programming tools for plotting data. http://CRAN.R-project.org/package=gplots

1003 Xu, Z., Chen, L., Leung, L., Yen, T.S., Lee, C., and Chan, J.Y. (2005). Liver-specific
1004 inactivation of the Nrf1 gene in adult mouse leads to nonalcoholic steatohepatitis and
1005 hepatic neoplasia. Proc Natl Acad Sci U S A 102:4120-5. doi:10.1073/pnas.0500660102

1006 Yang, F., Vought, B.W., Satterlee, J.S., Walker, A.K., Jim Sun, Z.Y., Watts, J.L.,
1007 DeBeaumont, R., Saito, R.M., Hyberts, S.G., Yang, S., et al. (2006). An ARC/Mediator
1008 subunit required for SREBP control of cholesterol and lipid homeostasis. Nature
1009 442:700-4. doi:10.1038/nature04942

1010 Yen, K., Le, T.T., Bansal, A., Narasimhan, S.D., Cheng, J.X., and Tissenbaum, H.A.
1011 (2010). A comparative study of fat storage quantitation in nematode Caenorhabditis
1012 elegans using label and label-free methods. PLoS One 5:e12810.
1013 doi:10.1371/journal.pone.0012810

1014 Zarse, K., Schmeisser, S., Groth, M., Priebe, S., Beuster, G., Kuhlow, D., Guthke, R.,
1015 Platzer, M., Kahn, C.R., and Ristow, M. (2012). Impaired insulin/IGF1 signaling extends
1016 life span by promoting mitochondrial L-proline catabolism to induce a transient ROS
1017 signal. Cell Metab 15:451-65. doi:10.1016/j.cmet.2012.02.013

1018 Zhang, P., Na, H., Liu, Z., Zhang, S., Xue, P., Chen, Y., Pu, J., Peng, G., Huang, X.,
1019 Yang, F., et al. (2012). Proteomic study and marker protein identification of
1020 Caenorhabditis elegans lipid droplets. Mol Cell Proteomics 11:317-28.
1021 doi:10.1074/mcp.M111.016345

1022 Zhu, L.J., Gazin, C., Lawson, N.D., Pages, H., Lin, S.M., Lapointe, D.S., and Green,
1023 M.R. (2010). ChIPpeakAnno: a Bioconductor package to annotate ChIP-seq and ChIP-
1024 chip data. BMC Bioinformatics 11:237. doi:10.1186/1471-2105-11-237

1025

Figures

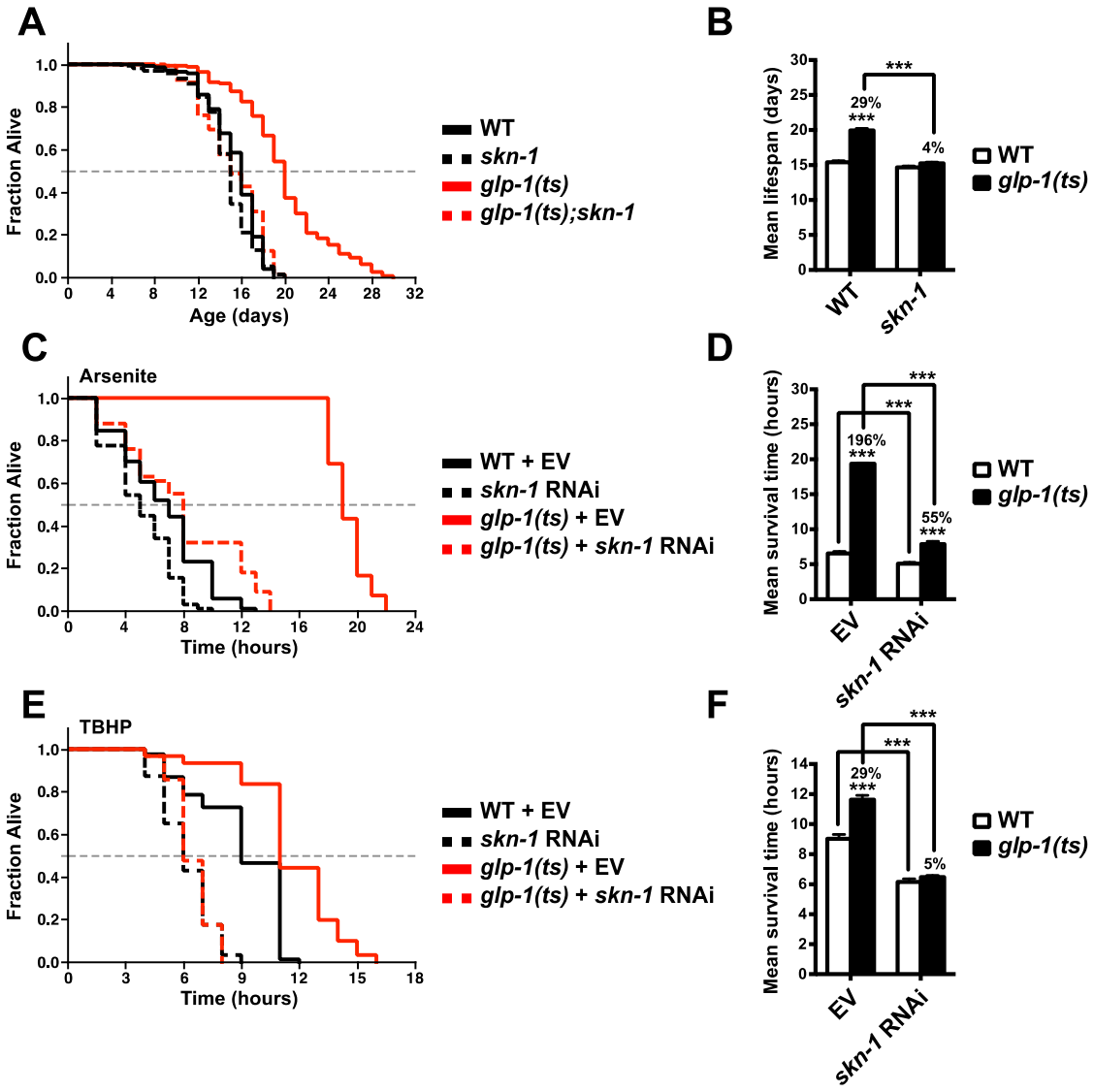

Figure 1. SKN-1 promotes longevity and stress resistance in GSC(-) animals. (A,B) Wild-type, *skn-1(zu135), glp-1(bn18ts)*, and *glp-1(bn18ts);skn-1(zu135)* double mutants were assayed for lifespan at 25°C. *skn-1(zu135)* is a presumed null that is used throughout the study. Unless otherwise specified, *glp-1(ts)* refers to *glp-1(bn18ts)*. (A) Composite survival curve. (B) Graph of mean lifespans. (C-F) *glp-1(ts)* mutants require *skn-1* for oxidative stress resistance. Day 3 adult *glp-1(ts)* and control worms treated with *skn-1* RNAi or empty vector were exposed to (C,D) 5 mM sodium arsenite (AS) or (E,F) 15.4 mM tert-butyl hydroperoxide (TBHP). Data are represented as mean ± SEM. $P < 0.001$***. The interaction between *glp-1* and *skn-1* was significant for both lifespan and stress resistance ($P < 0.001$). Statistical analysis and replicates are in **Tables 1 and 2**.

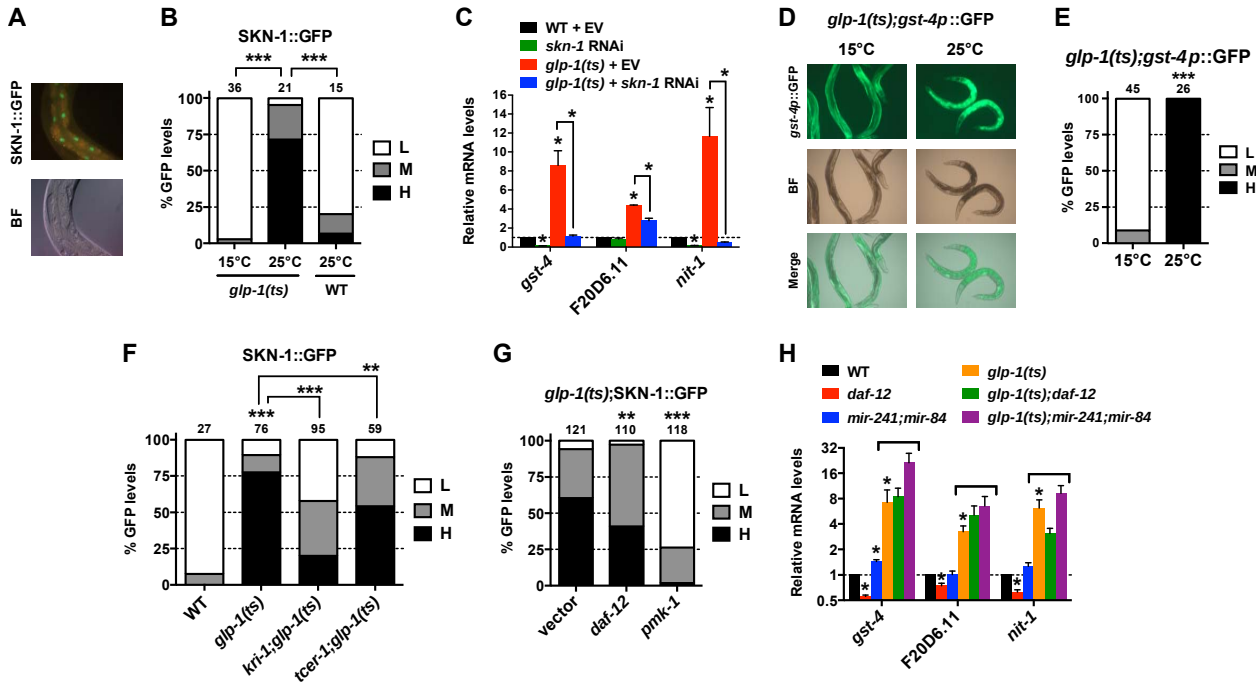

Figure 2. GSCs inhibit SKN-1 activity in the intestine. (A) Representative images of SKN-1::GFP in intestinal nuclei; GFP channel (top), bright field (BF; bottom). (B) Accumulation of SKN-1::GFP in intestinal nuclei in GSC(-) animals. (C) *skn-1*-dependent activation of direct SKN-1 target genes (Robida-Stubbs et al., 2012) in response to GSC absence, detected by qRT-PCR. (D,E) Increased expression of *gst-4p*::GFP in the intestine of *glp-1(ts)* animals. Hypodermal *gst-4p*::GFP expression appeared to be unaffected. (D) Representative 10X images. (E) Intestinal *gst-4p*::GFP quantification. (F-H) GSCs regulate SKN-1 parallel to DAF-16 and DAF-12. In (H), SKN-1 target genes are assayed by qRT-PCR. *glp-1(ts)* refers to *glp-1(e2141ts)*, and horizontal black lines indicate strains lacking GSCs. (C,H) Data are represented as mean ± SEM. n = 3 for qRT-PCR samples. (B,E,F,G) GFP quantification with high, medium, low scoring. Numbers above bars denote sample size. $P < 0.05$*; $P < 0.01$**; $P < 0.001$***.

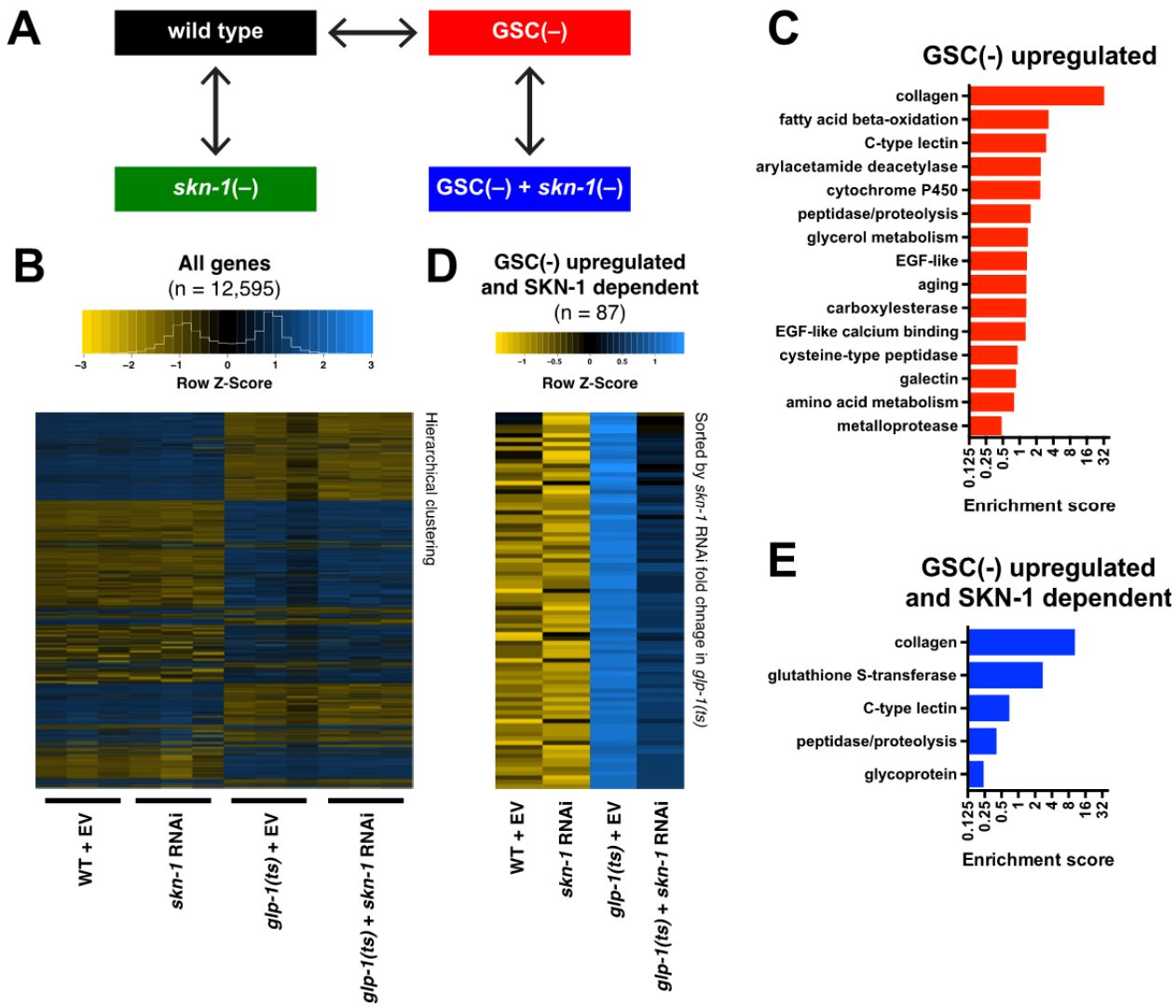

Figure 3. Effects of GSC absence and *skn-1* on gene expression. (A) RNA-seq experiment setup. For each condition, three biological replicates were obtained from synchronized intact day-one adults at 25°C. Arrows indicate comparisons that were made, and GSC(-) refers to *glp-1(ts)*. (B) Heatmap of all genes evaluated, showing biological replicates. (C) DAVID functional annotation analysis of GSC(-)-upregulated genes. (D) Heatmap of genes upregulated in *glp-1(ts)* in a *skn-1*-dependent manner (87 genes; FC > 4 in GSC(-); FC < 0.67 with *skn-1* RNAi in GSC(-)). (E) Functional annotation of the genes shown in (D). Genes and additional statistics are provided in **Supplementary files 1a-1d**.

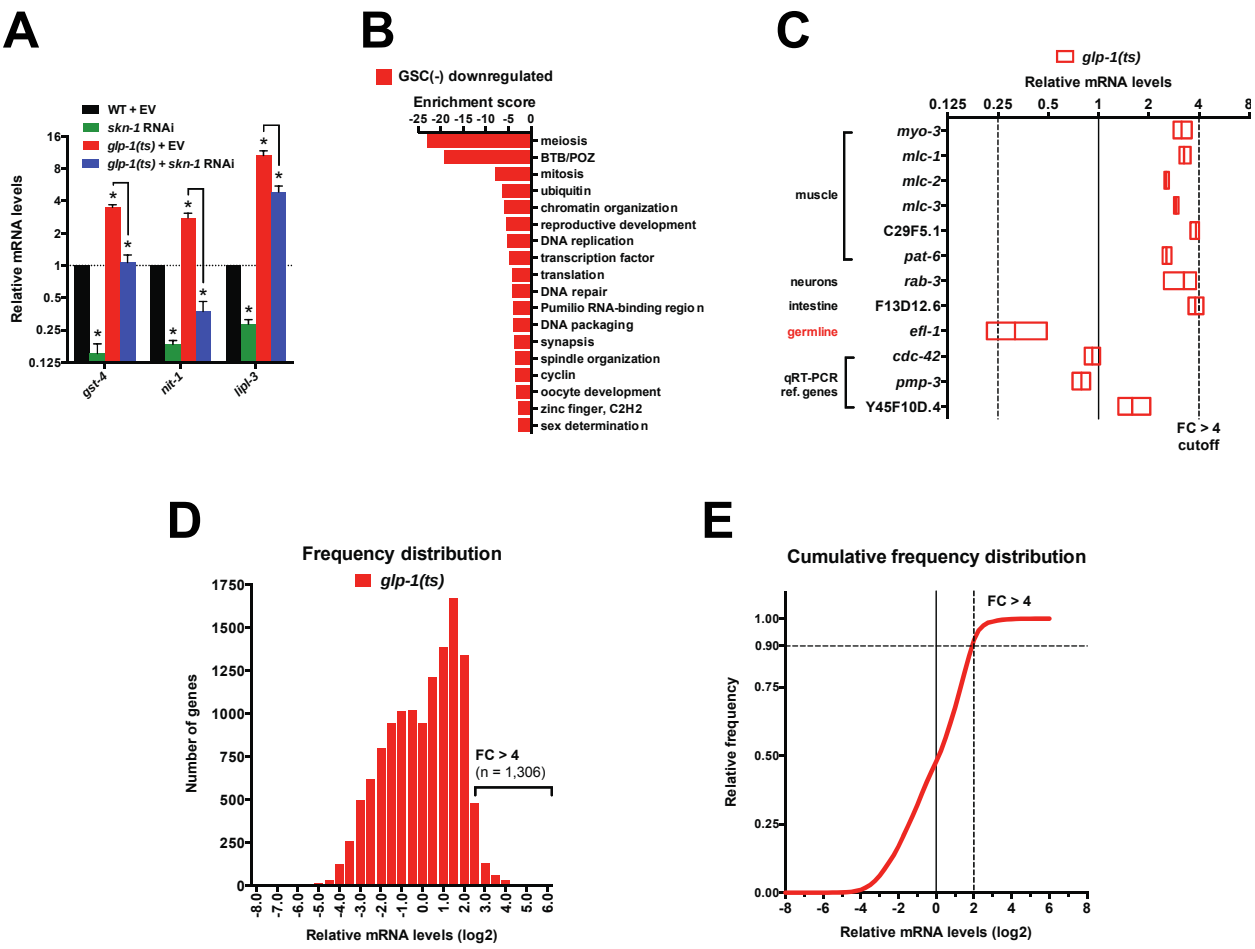

Figure 3–figure supplement 1. Gene expression changes following GSC inhibition. (A) qRT-PCR validation of RNA samples used for RNA-seq. *gst-4* and *nit-1* are direct SKN-1 targets (Robida-Stubbs et al., 2012). Data are represented as mean ± SEM. n = 3; $P < 0.05$*. Analysis of a different RNA sample set is shown in **Figure 2D**. (B) DAVID analysis of genes that were downregulated in *glp-1(ts)*. Processes related to GSC maintenance and reproduction were highly represented, as expected. (C) Altered abundance of tissue-specific genes in GSC(-) animals. Adult hermaphrodite worms have 959 somatic cells and ~2,000 GSCs (Kimble and Crittenden, 2005). A representative somatic-specific gene would therefore be predicted to be present at higher relative abundance in GSC(-) samples after normalization to either total RNA, or reference housekeeping genes. Accordingly, representative somatic tissue-specific genes (Richmond, 2005; Moerman and Williams, 2006; Chikina et al., 2009) were present at 3-4-fold higher relative levels in the GSC(-) samples. By contrast, a germline-specific gene (*efl-1*) was underrepresented (~4x) in GSC(-) samples. Reference genes that are ubiquitously expressed in all tissues and commonly used for qRT-PCR normalization (Hoogewijs et al., 2008) do not have altered relative abundance in the GSC(-) samples. (D,E) Frequency distribution plots of mRNA levels in *glp-1(ts)* worms relative to wild-type. A cutoff of FC > 4 denotes 1,306 out of 12,595 genes sequenced (10.4%).

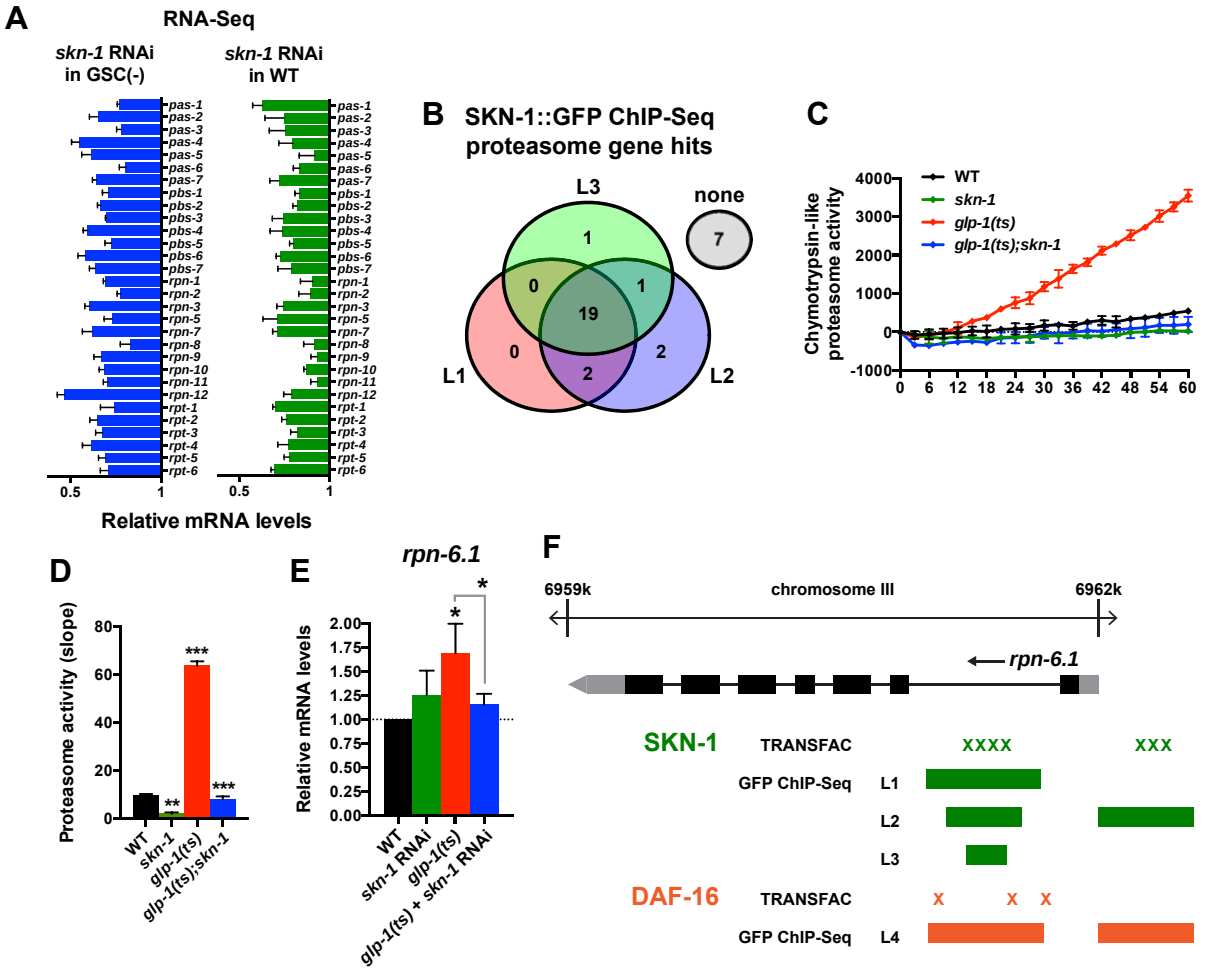

Figure 4. SKN-1 increases proteasome activity in response to GSC absence. (A) Reduction in relative proteasome gene subunit mRNA levels by *skn-1* RNAi, detected by RNA-seq. (B) Venn diagram indicating the number proteasome subunit genes (*pas*, *pbs*, *rpn*, *rpt* families) that have SKN-1::GFP ChIP-seq peak hits near the transcription start site at the indicated larval stage (Niu et al., 2011). (C, D) SKN-1-dependence of increased chymotrypsin-related proteasome activity in GSC-ablated worms. The slopes from (C) are graphed in (D). Additional experiments are in **Figure 4–figure supplement 1**. (E) SKN-1-dependence of *rpn-6.1* upregulation. Data are represented as mean ± SEM. n = 3 for all experiments. $P < 0.05$*; $P < 0.01$**; $P < 0.001$***. (F) Direct binding of SKN-1 and DAF-16 to the *rpn-6.1* gene, indicated by TRANSFAC transcription factor binding prediction and modENCODE GFP ChIP-seq analyses. Both the predicted promoter and first intron of *rpn-6.1* are highly enriched for SKN-1 and DAF-16 binding.

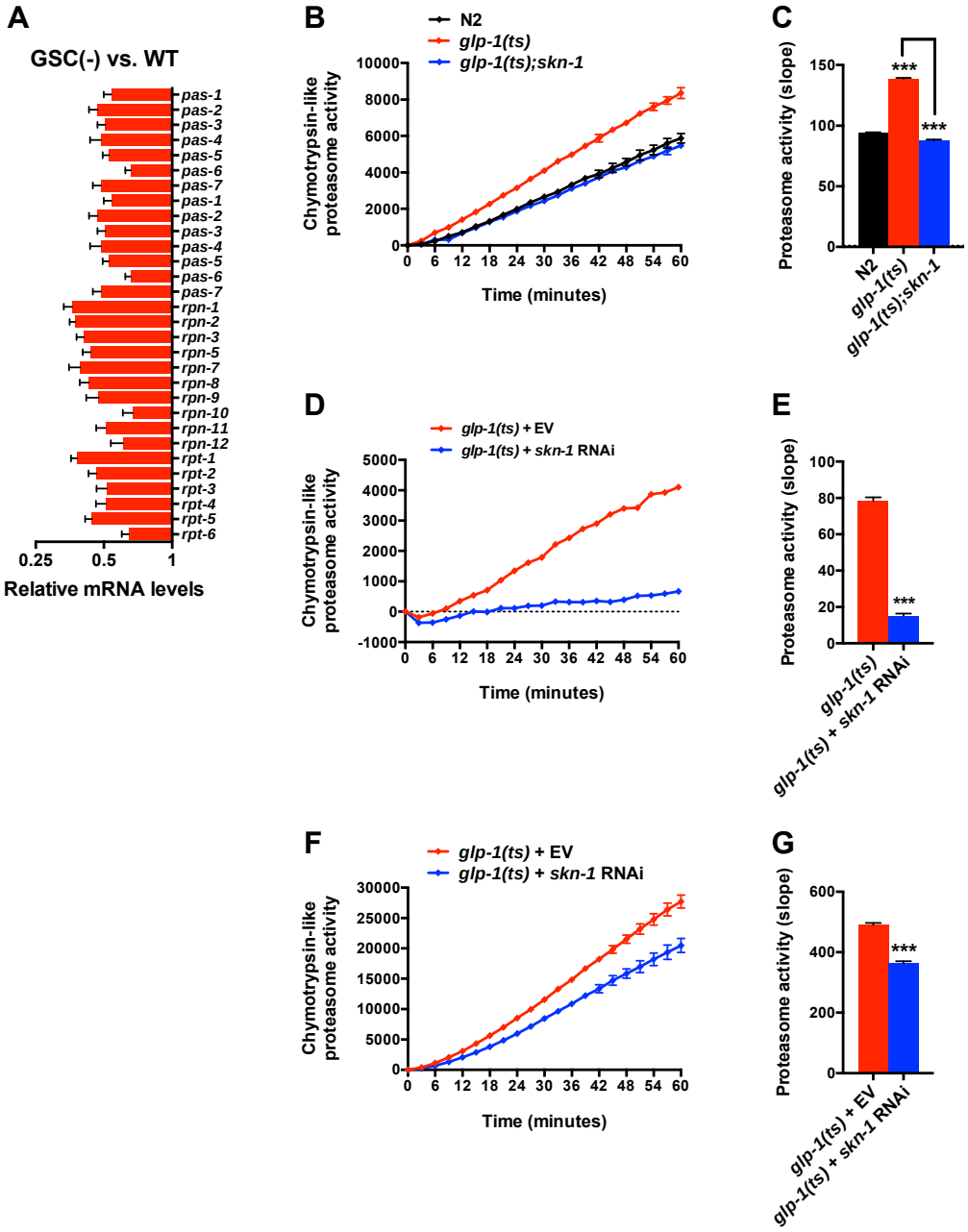

Figure 4–figure supplement 1. SKN-1-dependence of the increased proteasome activity in GSC(-) animals. (A) GSC absence reduces relative proteasome subunit gene mRNA abundance, detected by RNA-seq. (B,C) The *skn-1(zu135)* mutation suppresses the increase in 26S proteasome activity seen in day-one adult *glp-1(ts)* animals. (D,E) *skn-1* RNAi administered from the egg stage suppresses proteasome activity in day-one adult *glp-1(ts)* animals. (F,G) *skn-1* RNAi administered post-developmentally, starting at day 1 adulthood, significantly reduces proteasome activity in day 5 adult *glp-1(ts)* animals. (B,D,F) Kinetic curves of chymotrypsin-like proteasome activity. (C,E,G) Graphs of proteasome activity slopes. Data are represented as mean ± SEM. n = 3; $P < 0.001$***.

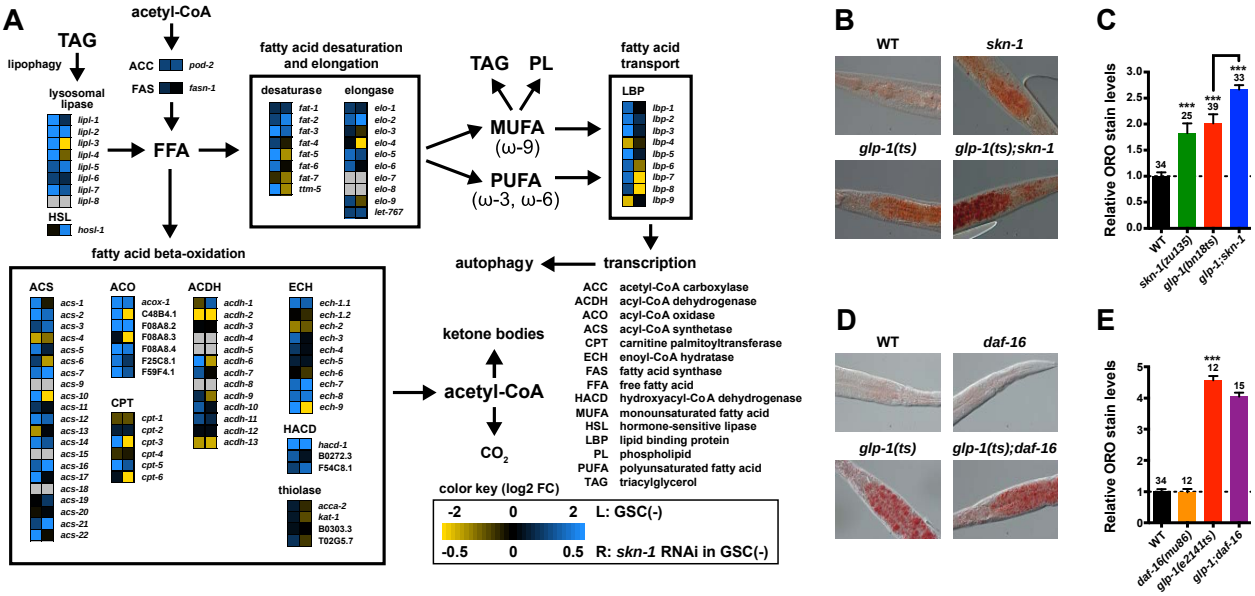

Figure 5. SKN-1 regulates lipid metabolism in GSC(-) animals. (A) Functional map of lipid metabolism gene expression. Left columns show the effects of GSC absence (GSC(-) vs WT), and right columns the effects of *skn-1* RNAi in GSC(-) animals. SKN-1 regulates genes involved in FA oxidation, breakdown of triacylglycerols (triglycerides, TAG) to free FAs, production of mono- and poly-unsaturated FAs (MUFA, PUFA), and FA transport. Color coding reflects relative representation in RNA-seq data, with blue and yellow indicating increased and decreased expression, respectively. (B-E) Increased fat levels in *glp-1(ts)* and *skn-1* mutants but not *daf-16* mutants. (D,E) *glp-1(ts)* refers to *glp-1(e2141ts)*. Representative 40X DIC images of fixed ORO-stained worms are shown in (B,D), with quantification provided in (C,E). Additional images and quantification are provided in **Figure 5–figure supplement 1**. Data are represented as mean ± SEM. Numbers above bars denote sample size. $P < 0.001$***.

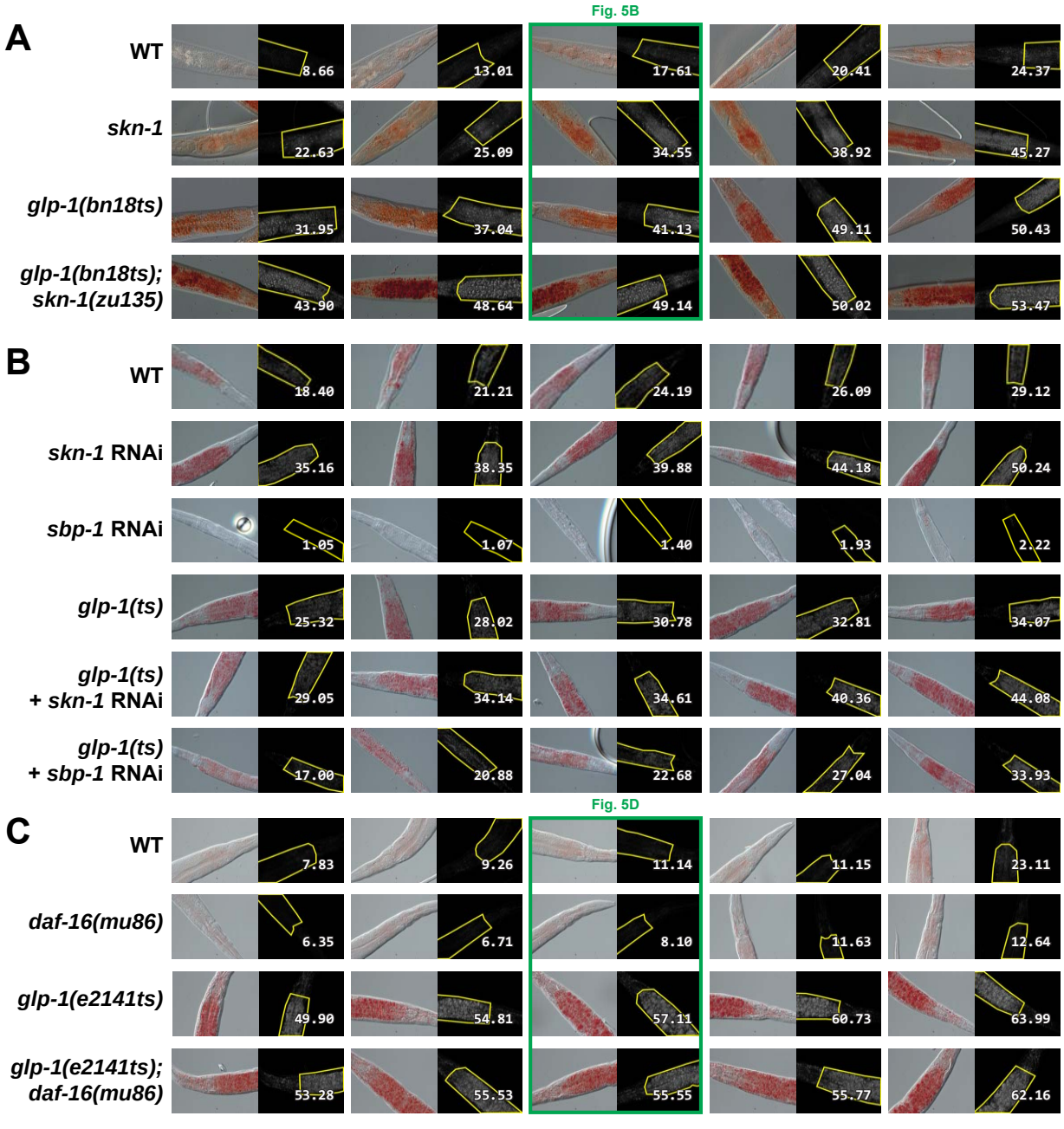

Figure 5–figure supplement 1. Representative ORO staining images with quantification. Representative images divided into approximate quintiles, ordered by mean pixel intensity, are shown for each strain. BF images are presented on the left and background subtracted images with quantification on the right. (A) *glp-1(bn18ts)* and *skn-1(zu135)* mutants. (B) *glp-1(ts)* mutants treated with *skn-1* and *sbp-1* RNAi. Increased staining was observed both with *skn-1* mutants and *skn-1* RNAi. RNAi against *sbp-1*, which is required for lipogenesis (Yang et al., 2006), decreases ORO staining in both WT and *glp-1(ts)* genetic backgrounds. (C) *glp-1(e2141ts)* and *daf-16(mu86)* mutants. Numbers indicate mean pixel intensity above background (see **Methods** for additional details).

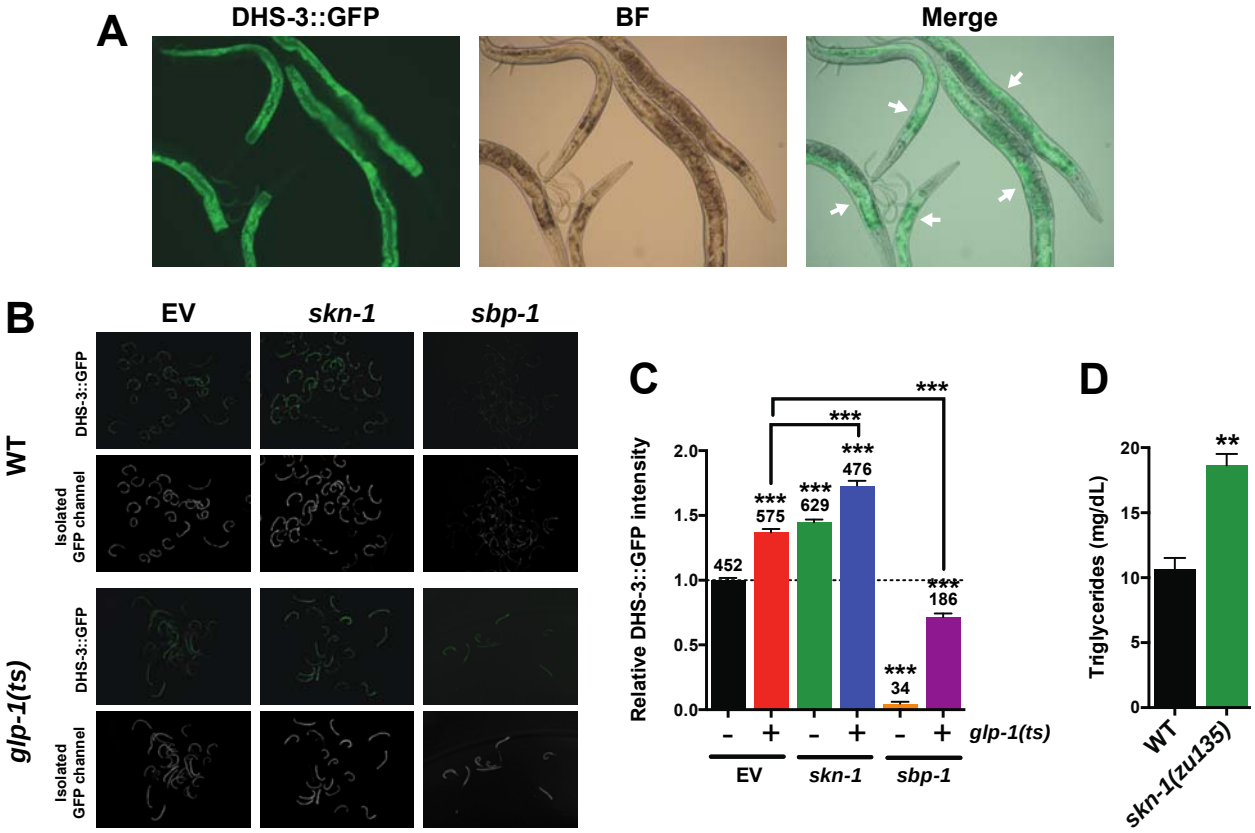

Figure 5–figure supplement 2. Analysis of the intestinal lipid droplet marker DHS-3::GFP, and triglyceride levels. *skn-1* RNAi increases DHS-3::GFP intensity in both wild-type and GSC(-) animals, whereas *sbp-1* RNAi decreases DHS-3::GFP intensity. (A) 10X slide mounted DHS-3::GFP images. White arrows indicate intestine-specific expression. (B,C) COPAS Biosorter quantification of DHS-3::GFP in live day-one adult worms. (B) Representative 10X inverted scope images of worms suspended in M9 buffer used for COPAS scoring. (C) Graph of mean DHS-3::GFP fluorescence, assayed by COPAS. Numbers above bars denote sample size. Asterisks directly above bars indicate *P* values relative to WT or RNAi control. Asterisks above black lines denote effect of RNAi in *glp-1(ts)* background. RNAi was started from egg stage and animals were raised at 25°C. (D) Triglyceride (TAG) levels are significantly elevated in *skn-1* mutants. Data are represented as mean ± SEM. $P < 0.01$**; $P < 0.001$***.

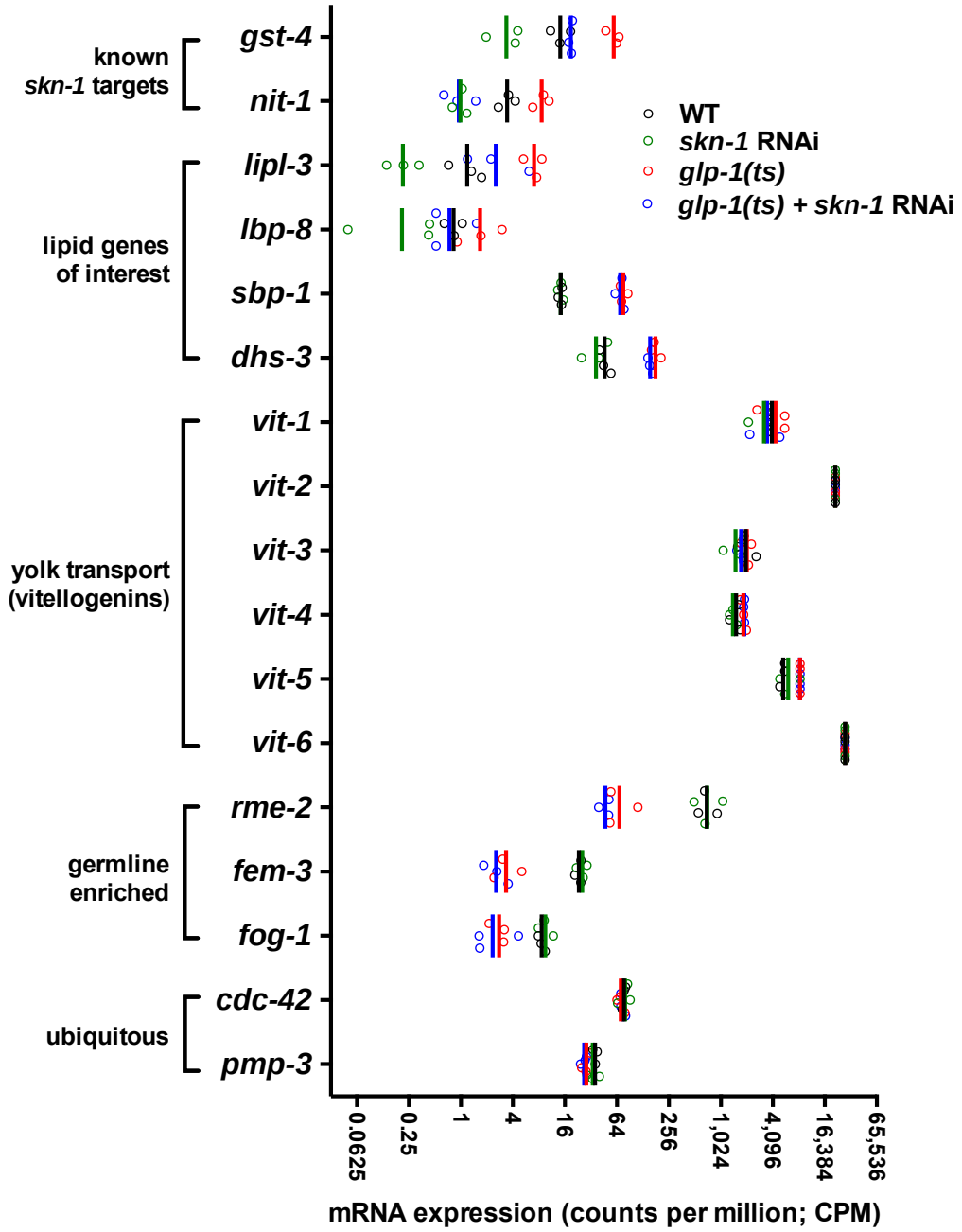

Figure 5–figure supplement 3. RNA-seq counts of select lipid metabolism and yolk transporter genes. Expression of the known SKN-1 target genes *gst-4* and *nit-1* are elevated in GSC(-) animals in a *skn-1*-dependent manner. The TAG lipase *lipl-3* and FABP *lbp-8* are similarly elevated in GSC(-) animals in a *skn-1*-dependent manner, but expression of *sbp-1*, *dhs-3*, and yolk protein vitellogenins (VIT genes) are not affected by *skn-1* RNAi. *rme-2* expression is germline enriched but regulated independently of *skn-1*. Open circles denote replicates. Vertical lines indicate mean counts per million (CPM).

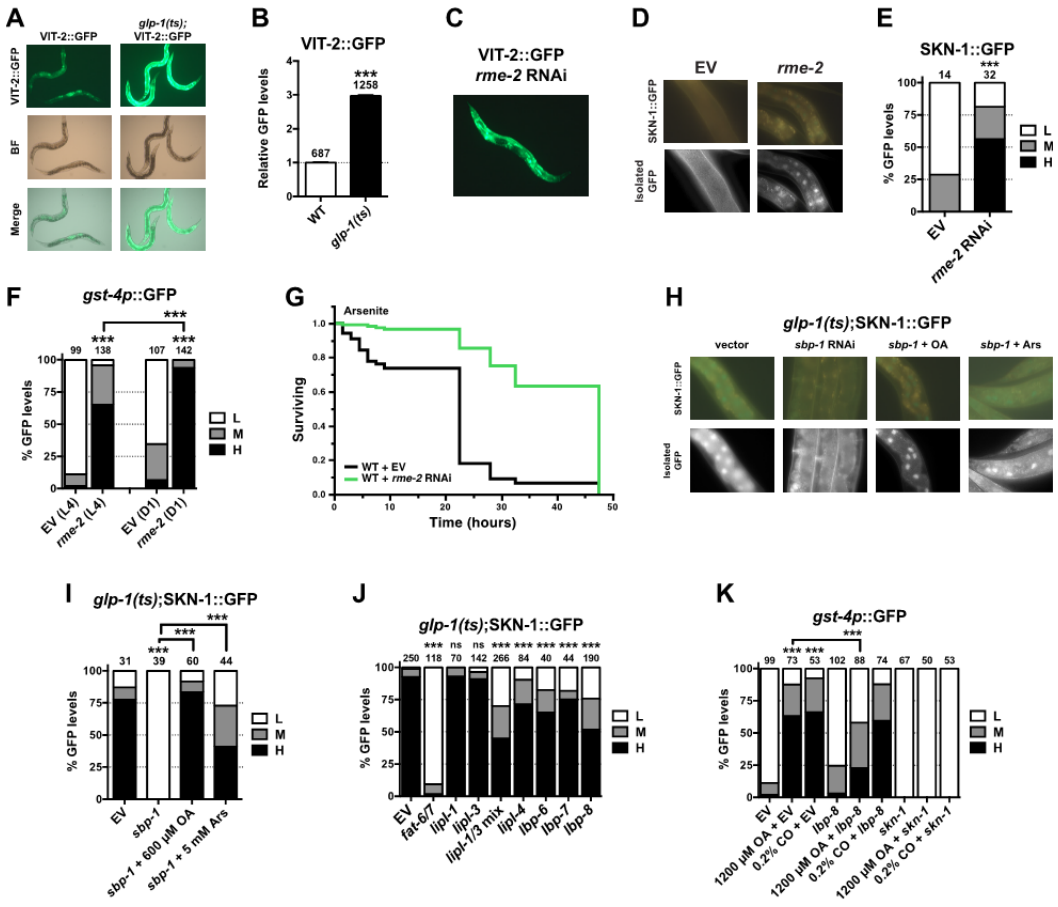

Figure 6. GSC absence activates SKN-1 through FA signaling. (A) Accumulation of yolk transporter vitellogenin (VIT-2::GFP) in the soma of GSC(-) animals. Detailed higher magnification images are provided in **Figure 6–figure supplement 1**. (B) COPAS quantification of VIT-2::GFP. Data are represented as mean ± SEM. (C) Knockdown of the oocyte-specific yolk receptor *rme-2* promotes somatic VIT-2 accumulation. (D-F) *rme-2* RNAi activates SKN-1 in the intestine. (D,E) SKN-1::GFP accumulates in intestinal nuclei in *rme-2* RNAi-treated worms. (F) In *rme-2* RNAi-treated worms, *gst-4p*::GFP levels in the intestine are increased at the L4 stage, and increased further by day 1 adulthood. (G) *rme-2* RNAi enhances resistance to AS, in a *skn-1*-dependent manner (see replicates in **Table 2**). (H,I) An OA-dependent signal is required for SKN-1 to be activated by GSC inhibition but not oxidative stress. In GSC(-) animals, SKN-1 nuclear accumulation is abolished by *sbp-1* RNAi, and rescued by OA supplementation. SKN-1 remains capable of responding to oxidative stress (30 min AS exposure) after *sbp-1* RNAi in GSC(-) (H,I) or WT (**Figure 6–figure supplement 2A**) worms. (J) Dependence of SKN-1::GFP accumulation in GSC(-) animals on FAT-6/7-mediated FA desaturation, and proteins that generate free unsaturated FAs (LIPL-1/-3 lipases), or transport them to the nucleus (LBP-6/7/8). (K) OA and CO increase *skn-1*-dependent *gst-4*p::GFP expression in the intestine. *lbp-8* RNAi reduces induction by OA. (A,C) Representative 10X GFP images. (D,H) Representative 40X GFP images of day-one adults. (E,F,I-K) GFP quantification with high, medium, low scoring. Numbers above bars denote sample size. $P < 0.001$***.

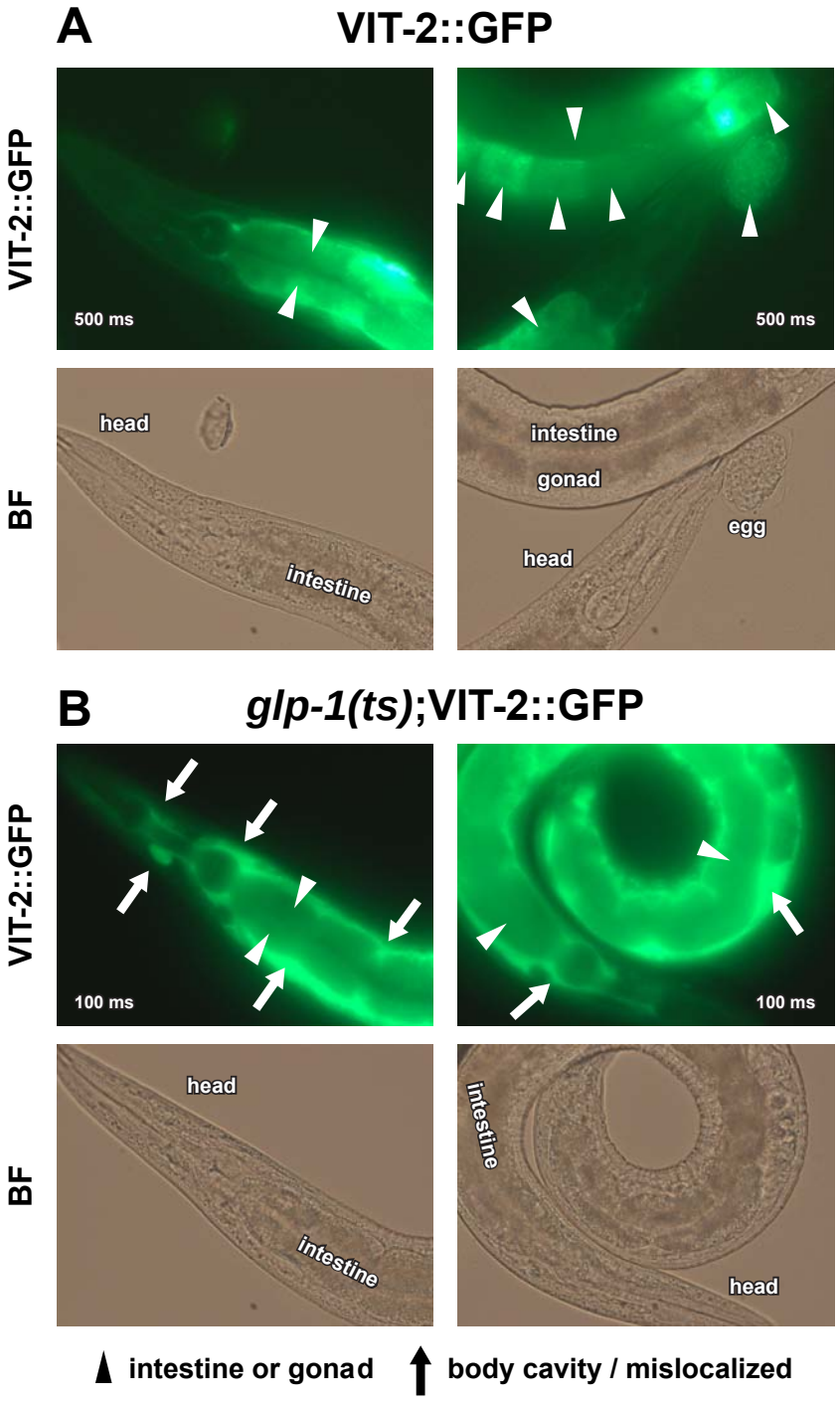

1177

1178 **Figure 6–figure supplement 1. Enlarged VIT-2::GFP images.** 40X GFP and BF
1179 images of (A) GSC(+) and (B) GSC(-) animals are shown. Note that *glp-1(ts);*VIT-
1180 2::GFP are presented with 5x lower exposure times due to increased VIT-2::GFP
1181 intensity in GSC(-) animals. All worms shown are day-one adults raised at 25°C.
1182 Arrowheads indicate the normal distribution of VIT-2::GFP in the intestine and oocytes,
1183 and arrows indicate the ectopic accumulation of VIT-2::GFP seen in GSC(-) animals.
1184 Numbers superimposed on images denote GFP exposure times.

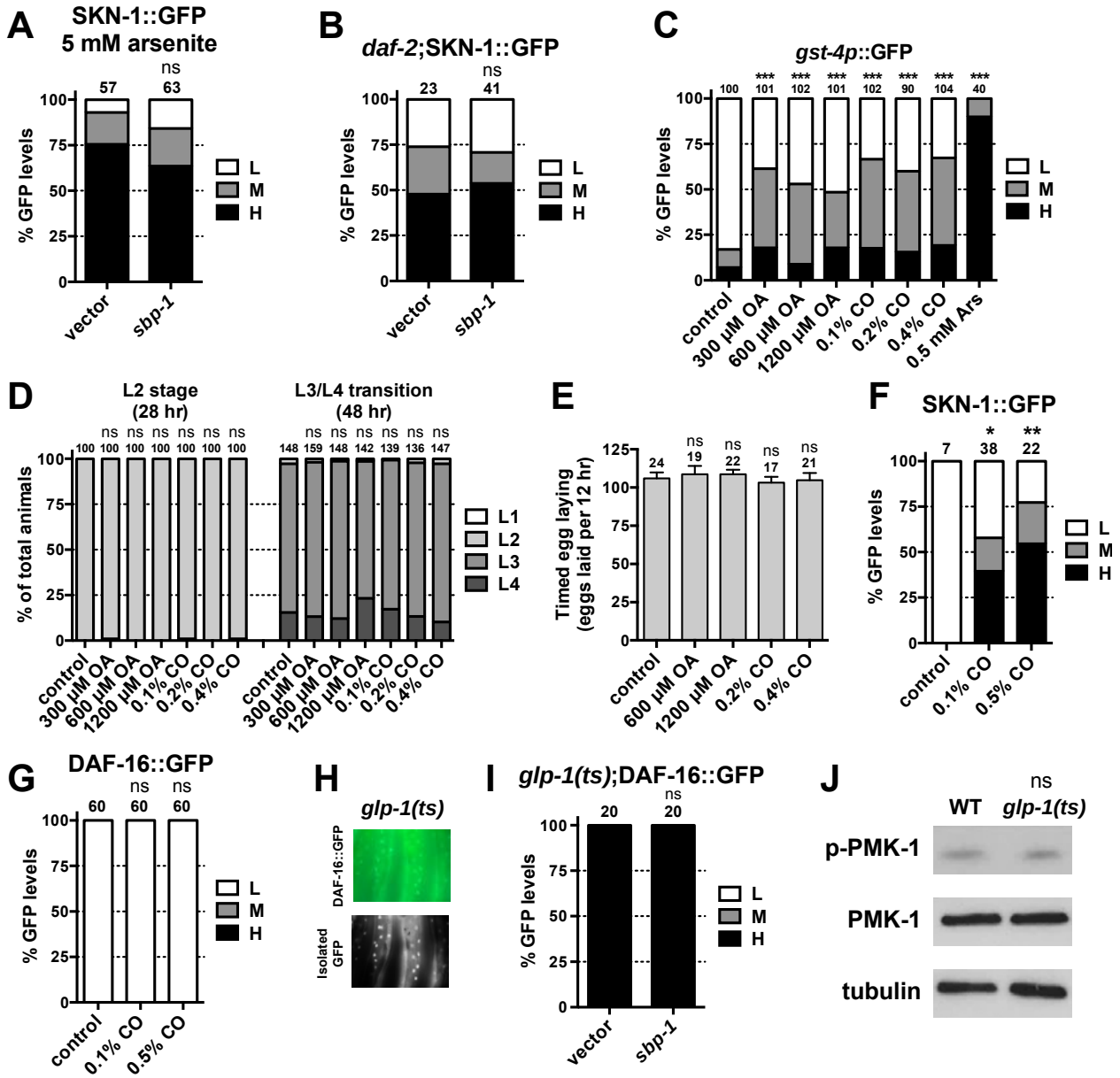

Figure 6–figure supplement 2. SKN-1 is activated in response to FA signaling. Accumulation of SKN-1 in intestinal nuclei in (A) response to arsenite (AS) exposure for 30 min or (B) *daf-2* mutants is not impaired by *sbp-1* RNAi. (C) Effects of oleic acid (OA) and coconut oil (CO) doses on intestinal *gst-4p*::GFP expression, compared to AS treatment. (D) Larval development and (E) egg laying rate are not affected by OA or CO treatment. CO supplementation induces intestinal (F) SKN-1 nuclear accumulation but not (G) DAF-16 accumulation. (H,I) DAF-16 accumulation in *glp-1(e2141ts)* is unaffected by *sbp-1* RNAi. (H) Representative 40X DIC images of day-one adults. (J) PMK-1 (p38 kinase) phosphorylation is not affected by GSC removal, consistent with a previous report (Alper et al., 2010). PMK-1 phosphorylation is increased dramatically by AS oxidative stress, and reflects activation of its kinase activity (Inoue et al., 2005). (A-C,F,G,I) GFP quantification with high, medium, low scoring. Numbers above bars denote sample size. $P < 0.05$*; $P < 0.01$**; $P < 0.001$***.

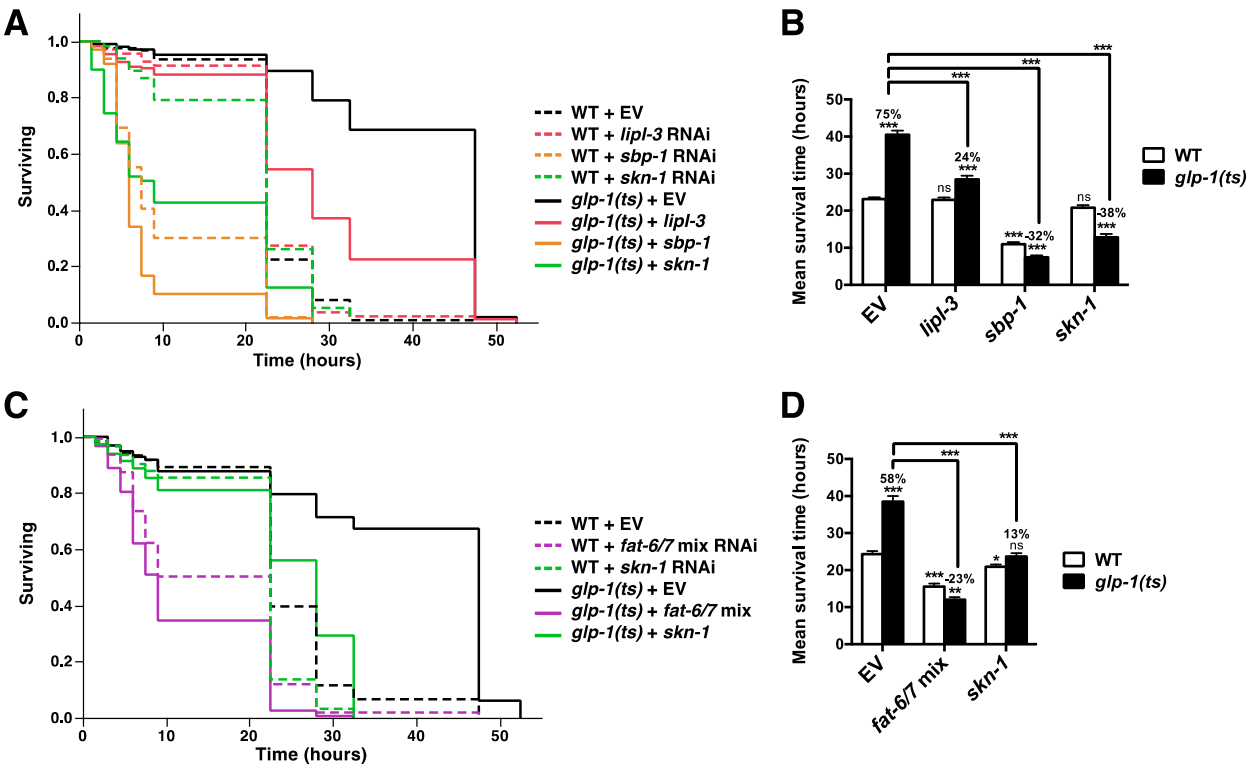

Figure 6–figure supplement 3. Fatty acid desaturation is required for GSC(-) stress resistance. *glp-1(ts)* and control day-one adult worms treated with *lipl-3*, *sbp-1*, *fat-6/7* mix, *skn-1,* or empty vector RNAi were exposed to 5 mM AS. Knockdown of *lipl-3* (A,B), and either *sbp-1* (A,B) or *fat-6/7* (C,D) abolished the increase in AS resistance seen in *glp-1(ts)* animals. (B,D) Data are represented as mean ± SEM. $P < 0.05$*; $P < 0.01$**; $P < 0.001$***. The interaction between *glp-1(ts)* and *fat-6/7*, *lipl-3*, *sbp-1*, and *skn-1* were significant ($P < 0.001$). Additional information and statistics are provided in **Table 2.**

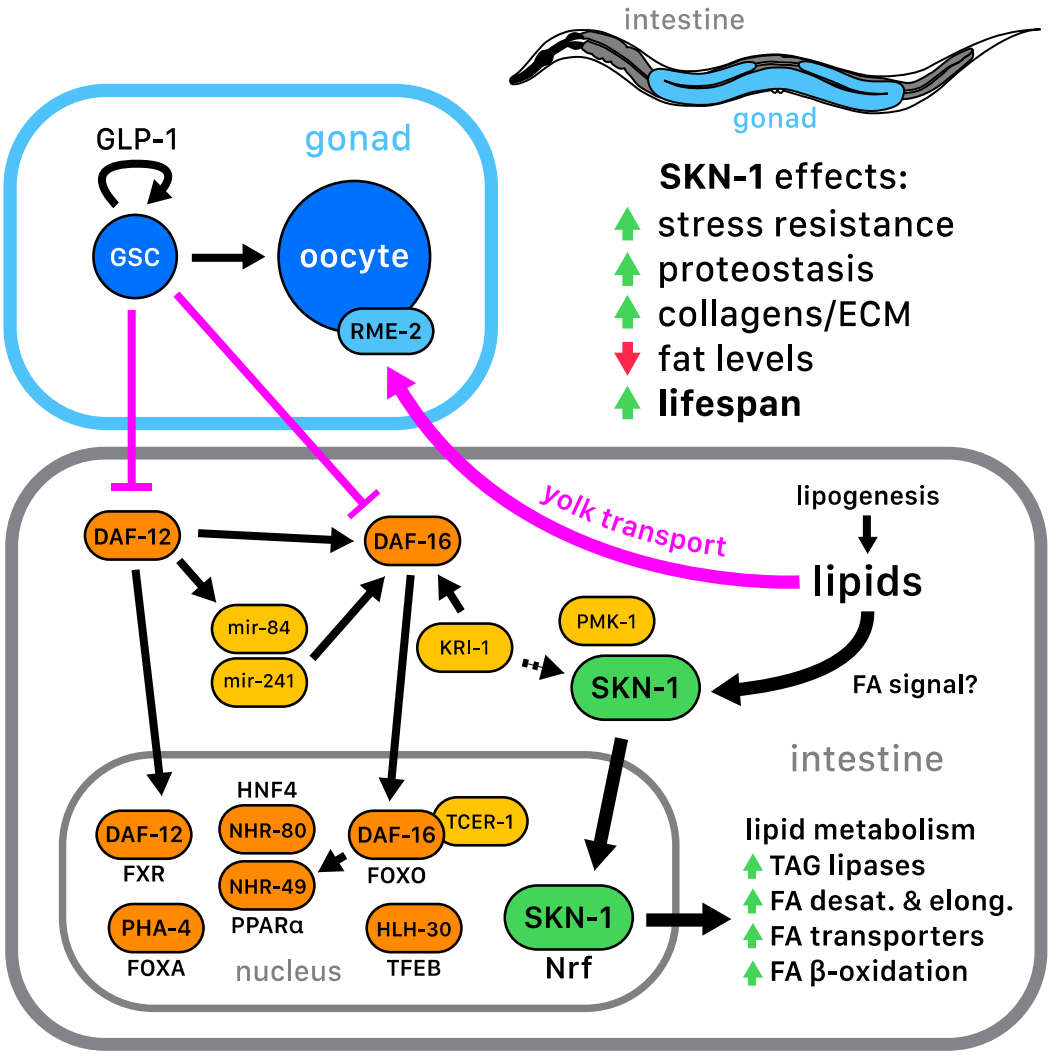

Figure 7. SKN-1 regulation in the GSC longevity pathway. GSC absence results in activation of transcription factors in the intestine, with SKN-1 being regulated in parallel to DAF-12 and DAF-16. Yolk transport to oocytes is disrupted by GSC loss, resulting in lipid accumulation in the intestine and body cavity. The resulting SKN-1 activation requires OA, the FAT-6/7 FA desaturases, and the lysosomal lipases LIPL-1/3. This lipid-based signaling to SKN-1 depends partially upon LBP-8, which transports FAs from the lysosome to the nucleus. SKN-1 induces transcription of genes involved in stress resistance, detoxification, proteasome maintenance, extracellular matrix, and lipid metabolism, thereby reducing fat storage, and increasing stress resistance and lifespan. Magenta denotes processes that are active in the presence of GSCs.

Tables

Set	Strain	Mean Lifespan ± SEM (days)	Median Lifespan (days)	75th % (days)	N	% Mean Lifespan Ext.	*P* value (log-rank) vs. N2 * vs. *glp-1* †
Lifespan at 25°C							
Composite lifespan at 25°C with FUdR (from 2 replicates)							
C1	N2	15.40 ± 0.2	16	17	133/148	-	-
	skn-1(zu135)	14.66 ± 0.2	15	16	158/167	-	-
	glp-1(bn18ts)	19.94 ± 0.3	20	22	164/171	29.48	< 0.0001*
	glp-1(bn18ts);skn-1(zu135)	15.23 ± 0.2	15	18	149/170	3.89	< 0.0001†
				two-way ANOVA *glp-1(ts)* and *skn-1* interaction			< 0.0001
Replicate lifespans at 25°C with FUdR							
#1	N2	13.99 ± 0.4	14	17	40/55	-	-
	skn-1(zu135)	12.54 ± 0.3	13	14	41/50	-	-
	glp-1(bn18ts)	22.46 ± 0.8	25	27	50/55	60.54	< 0.0001*
	glp-1(bn18ts);skn-1(zu135)	13.29 ± 0.4	12	14	53/70	6.00	< 0.0001†
					glp-1(ts) and *skn-1* interaction		< 0.0001
#2	N2	16.07 ± 0.2	16	17	93/93	-	-
	skn-1(zu135)	15.42 ± 0.2	15	17	117/117	-	-
	glp-1(bn18ts)	18.86 ± 0.3	19	21	114/116	17.36	< 0.0001*
	glp-1(bn18ts);skn-1(zu135)	16.42 ± 0.2	17	18	96/100	6.49	< 0.0001†
					glp-1(ts) and *skn-1* interaction		0.0002
Lifespan at 20°C **(25°C during development, downshifted to 20°C at D1 adulthood)**							
Lifespan at 20°C without FUdR							
#3	N2	20.36 ± 0.6	18	21	42/50	-	-
	skn-1(zu135)	18.39 ± 0.5	18	18	27/47	-	-
	glp-1(bn18ts)	25.87 ± 1.3	24	33	35/66	27.06	0.0002*
	glp-1(bn18ts);skn-1(zu135)	20.02 ± 0.6	18	24	34/55	8.86	< 0.0001†
					glp-1(ts) and *skn-1* interaction		0.0230
Composite lifespan at 20°C with FUdR (from 2 replicates)							
C2	N2	20.51 ± 0.5	21	24	86/90	-	-
	skn-1(zu135)	17.78 ± 0.4	19	20	88/94	-	-
	glp-1(bn18ts)	24.52 ± 0.6	25	28	81/104	19.55	< 0.0001*
	glp-1(bn18ts);skn-1(zu135)	20.47 ± 0.5	20	24	91/98	15.13	< 0.0001†
					glp-1(ts) and *skn-1* interaction		0.1892
Replicate lifespans at 20°C with FUdR							
#4	N2	18.09 ± 0.4	17	19	33/37	-	-
	skn-1(zu135)	14.78 ± 0.5	14	17	31/35	-	-
	glp-1(bn18ts)	21.79 ± 1.0	21	28	28/50	20.45	0.0002*
	glp-1(bn18ts);skn-1(zu135)	16.83 ± 0.3	17	18	36/43	13.87	< 0.0001†
					glp-1(ts) and *skn-1* interaction		0.1491
#5	N2	22.00 ± 0.6	23	25	53/53	-	-
	skn-1(zu135)	19.40 ± 0.4	20	21	57/59	-	-
	glp-1(bn18ts)	25.91 ± 0.7	25	30	53/54	17.77	< 0.0001*
	glp-1(bn18ts);skn-1(zu135)	22.80 ± 0.6	24	26	55/55	17.53	< 0.0001†
					glp-1(ts) and *skn-1* interaction		0.6607

Table 1. Lifespans. Percent lifespan extension refers to *glp-1(ts)* versus wild-type or *skn-1* control. *P* values were calculated by log-rank test. The interaction effect of *glp-1(ts)* and *skn-1* were calculated by two-way ANOVA using mean lifespan. The last *P* value reflects the specific requirement of *skn-1* for *glp-1(ts)* lifespan, as opposed to its

effect on lifespan in general. Homozygous *skn-1* mutants produce eggs that do not hatch because of a catastrophic defect in developmental patterning, but do not exhibit known defects in the germline itself (Bowerman et al., 1992).

Set	Strain	Mean Survival ± SEM (hrs)	Median Survival (hrs)	75th % Survival (hrs)	N	% Mean Survival Ext.	*P* value vs. N2 * vs. *glp-1* † vs. *rme-2* ‡
Sodium arsenite (day 1 adulthood) **25°C continuous; RNAi from L1**							
#1	N2 + vector RNAi	20.20 ± 1.0	22.5	22.5	122/122	-	-
	N2 + *rme-2* RNAi	39.51 ± 1.1	47.5	47.5	117/117	95.59	< 0.0001*
#2	N2 + vector RNAi	26.82 ± 1.2	28.0	28.0	57/57	-	-
	N2 + *rme-2* RNAi	53.21 ± 0.9	52.5	71.5	252/252	98.44	< 0.0001*
	glp-1(bn18ts) + vector RNA	53.06 ± 1.0	52.5	71.5	216/216	97.85	< 0.0001*
#3	N2 + vector RNAi (**20°C**)	38.59 ± 0.6	47.5	47.5	281/281	-	-
	N2 + *rme-2* RNAi	63.00 ± 0.7	71.5	71.5	287/287	63.25	< 0.0001*
#4	N2 + vector RNAi (**20°C**)	49.10 ± 0.8	46.0	64.0	306/306	-	-
	N2 + vector/*skn-1* mix RNAi	32.03 ± 0.6	40.0	40.0	271/271	-	-
	N2 + vector/*rme-2* mix RNAi	65.38 ± 1.1	64.0	70.0	361/361	33.16	< 0.0001*
	N2 + *rme-2*/*skn-1* mix RNAi	33.76 ± 0.5	40.0	40.0	409/409	5.40	< 0.0001‡
					two-way ANOVA *rme-2* and *skn-1* interaction		< 0.0001
#5	N2 + vector RNAi	23.18 ± 0.5	22.5	22.5	125/125	-	-
	N2 + *lipl-3* RNAi	23.04 ± 0.6	22.5	28.0	139/139	-	-
	N2 + *sbp-1* RNAi	11.01 ± 0.6	7.5	22.5	163/163	-	-
	N2 + *skn-1* RNAi	20.88 ± 0.7	22.5	28.0	115/115	-	-
	glp-1(bn18ts) + vector RNAi	40.58 ± 1.1	47.5	47.5	105/105	75.05	< 0.0001*
	glp-1(bn18ts) + *lipl-3* RNAi	28.52 ± 1.0	28.0	32.5	178/178	23.77	< 0.0001†
	glp-1(bn18ts) + *sbp-1* RNAi	7.50 ± 0.5	6.0	7.5	138/138	-31.88	< 0.0001†
	glp-1(bn18ts) + *skn-1* RNAi	12.90 ± 0.9	9.0	22.5	129/129	-38.21	< 0.0001†
						glp-1(ts) and *lipl-3* interaction	< 0.0001
						glp-1(ts) and *sbp-1* interaction	< 0.0001
						glp-1(ts) and *skn-1* interaction	< 0.0001
#6	N2 + vector RNAi	24.36 ± 0.8	22.5	28.0	121/121	-	-
	N2 + *fat-6/7* mix RNAi	15.56 ± 0.8	22.5	22.5	159/159	-	-
	N2 + *skn-1* RNAi	20.94 ± 0.6	22.5	22.5	124/124	-	-
	glp-1(bn18ts) + vector RNAi	38.49 ± 1.5	47.5	47.5	98/98	58.03	< 0.0001*
	glp-1(bn18ts) + *fat-6/7* mix RNAi	12.04 ± 0.7	9.0	22.5	153/153	-22.66	< 0.0001†
	glp-1(bn18ts) + *skn-1* RNAi	23.69 ± 0.9	28.0	32.5	116/116	13.13	< 0.0001†
						glp-1(ts) and *fat-6/7* interaction	< 0.0001
						glp-1(ts) and *skn-1* interaction	< 0.0001
Sodium arsenite (day 3 adulthood) **25°C during development, 20°C from D1; RNAi from D1**							
#7	N2 + vector RNAi	6.55 ± 0.3	7.0	8.0	104/104	-	-
	N2 + *skn-1* RNAi	5.08 ± 0.2	5.0	7.0	103/103	-	-
	glp-1(bn18ts) + vector RNAi	19.36 ± 0.1	19.0	20.0	97/97	195.57	< 0.0001*
	glp-1(bn18ts) + *skn-1* RNAi	7.86 ± 0.4	8.0	12.0	100/100	54.72	< 0.0001†
						glp-1(ts) and *skn-1* interaction	< 0.0001
#8	N2 + vector RNAi	8.31 ± 0.4	9.0	10.0	98/98	-	-
	N2 + *skn-1* RNAi	6.89 ± 0.3	8.0	9.0	90/90	-	-
	glp-1(bn18ts) + vector RNAi	16.95 ± 1.0	20.0	26.0	81/81	103.97	< 0.0001*
	glp-1(bn18ts) + *skn-1* RNAi	9.90 ± 0.4	10.0	12.0	91/91	43.69	< 0.0001†
						glp-1(ts) and *skn-1* interaction	< 0.0001
TBHP (day 3 adulthood) **25°C during development, 20°C from D1; RNAi from D1**							
#9	N2 + vector RNAi	9.02 ± 0.3	9.0	11.0	84/108	-	-
	N2 + *skn-1* RNAi	6.16 ± 0.2	6.0	7.0	63/98	-	-
	glp-1(bn18ts) + vector RNAi	11.62 ± 0.3	11.0	13.0	61/61	28.82	< 0.0001*
	glp-1(bn18ts) + *skn-1* RNAi	6.48 ± 0.1	8.0	7.0	63/65	5.19	< 0.0001†
						glp-1(ts) and *skn-1* interaction	< 0.0001
#10	N2	4.29 ± 0.2	4.0	4.0	65/94	-	-
	skn-1(zu135)	4.51 ± 0.1	5.0	3.0	73/74	-	-
	glp-1(bn18ts)	6.25 ± 0.2	6.0	4.0	73/74	45.69	< 0.0001*
	glp-1(bn18ts);skn-1(zu135)	4.78 ± 0.1	5.0	4.0	73/75	5.99	< 0.0001†
						glp-1(ts) and *skn-1* interaction	< 0.0001

Table 2. Stress resistance assays. Survival after sodium arsenite or TBHP treatment was assayed in adult animals. The increase in oxidative stress resistance of *glp-1(ts)* (GSC(-)) animals was impaired by loss of *fat-6/7*, *lipl-3*, *sbp-1*, and *skn-1*. Representative assays are shown. Percent survival extension refers to *glp-1(ts)* or *rme-2* RNAi vs. the matching wild-type or *skn-1* control. *P* values were calculated by log-rank test. The interaction effect of GSC(-) or *rme-2* with *skn-1*, or *fat-6/7*, *lipl-3*, and *sbp-1* were calculated by two-way ANOVA using mean lifespan. The last *P* value reflects the specific requirement of each gene for GSC(-) or *rme-2* stress resistance as opposed to its effect on stress resistance in general.

Code	Genetic Background	Transgene	Reference
AA003	*daf-12(rh61rh411)* X	–	(Shen et al., 2012)
AA983	*glp-1(e2141ts)* III; *daf-12(rh61rh411)* X	–	(Shen et al., 2012)
AA1049	*mir-241(n4315)* V; *mir-84(n4037)* X	–	(Shen et al., 2012)
AA1709	*glp-1(e2141ts)* III; *mir-241(n4315)* V; *mir-84(n4037)* X	–	(Shen et al., 2012)
AA2735	*glp-1(e2141ts)* III	–	(Shen et al., 2012)
CF1903	*glp-1(e2141ts)* III	–	(Berman and Kenyon, 2006)
CF1935	*daf-16(mu86)* I; *glp-1(e2141ts)* III	muIs109[*daf-16p::GFP::DAF-16* + *odr-1p::RFP*] X	(Berman and Kenyon, 2006)
CL2166	N2	dvIs19[pAF15(*gst-4p::GFP::NLS*)] III	(Link and Johnson, 2002)
DH1033	*sqt-1(sc103)* II	bIs1[*vit-2p::VIT-2::GFP* + *rol-6(su1006)*] X	(Grant and Hirsh, 1999)
EU31	*skn-1(zu135)* IV	–	(Bowerman et al., 1992)
LD001	N2	ldIs7[*SKN-1b/c::GFP* + *rol-6(su1006)*]	(An and Blackwell, 2003)
LD002	N2	ldIs1[*SKN-1b/c::GFP* + *rol-6(su1006)*]	(An and Blackwell, 2003)
LD1025	*daf-2(e1370)* III	ldIs7[*SKN-1b/c::GFP* + *rol-6(su1006)*]	(Tullet et al., 2008)
LD1425	*glp-1(bn18ts)* III	ldIs1[*SKN-1b/c::GFP* + *rol-6(su1006)*]	This study
LD1434	*glp-1(bn18ts)* III; *skn-1(zu135)* IV	–	This study
LD1473	*kri-1(ok1251)* I; *glp-1(bn18ts)* III	ldIs1[*SKN-1b/c::GFP* + *rol-6(su1006)*]	This study
LD1474	*tcer-1(tm1452)* II; *glp-1(bn18ts)* III	ldIs1[*SKN-1b/c::GFP* + *rol-6(su1006)*]	This study
LD1548	N2	ls[*dhs-3p::DHS-3::GFP*] I	(Zhang et al., 2012)
LD1549	*glp-1(bn18ts)* III	ls[*dhs-3p::DHS-3::GFP*] I	This study
LD1644	*sqt-1(sc103)* II; *glp-1(bn18ts)* III	bIs1[*vit-2p::VIT-2::GFP* + *rol-6(su1006)*] X	This study
LD1653	*glp-1(bn18ts)* III	–	(Dorsett et al., 2009) Outcrossed from DG2389
LD1744	*glp-1(bn18ts)* III	ldEx119[pAF15(*gst-4p::GFP::NLS*) + *rol-6(su1006)*]	This study
TJ356	N2	zIs356[*daf-16p::DAF-16a/b::GFP* + *rol-6*] IV	(Henderson and Johnson, 2001)

Table 3. *C. elegans* strains used in this study.

Gene	Sequence	Annotation	Primer pair
gst-4	K08F4.7	Glutathione S-transferase	FWD: CCCATTTTACAAGTCGATGG REV: CTTCCTCTGCAGTTTTTCCA
F20D6.11	F20D6.11	Flavin-adenine dinucleotide (FAD)-binding oxidoreductase	FWD: GGAAATTCTCGGTAGAATCGAA REV: ACGATCACGAACTTCGAACA
nit-1	ZK1058.6	Nitrilase	FWD: AATCCTCCGACTATCCCTTG REV: AGCGAATCGTTTCTTTTGTG
rpn-6.1	F57B9.10	19S non-ATPase subunit	FWD: AATATTGGAAAAGCACCTGAAATGT REV: TTTGATGTGGAAGTGAAGTCATTGT
lipl-3	R11G11.14	Lysosomal triglyceride lipase	FWD: ATGGGCAGGCAAATCCACCA REV: AGTTGTTCTGCGCAATTATA
**cdc-42*	R07G3.1	Housekeeping gene	FWD: CTGCTGGACAGGAAGATTACG REV: CTCGGACATTCTCGAATGAAG
*Y45F10D.4	Y45F10D.4	Housekeeping gene	FWD: GTCGCTTCAAATCAGTTCAGC REV: GTTCTTGTCAAGTGATCCGACA

Table 4. qRT-PCR primers used in this study. Select primer sequences were obtained from previous publications (Robida-Stubbs et al., 2012; Vilchez et al., 2012; O'Rourke and Ruvkun, 2013).

Supplementary files

[see Supplementary files 1-4.xlsx file]

Supplementary file 1a. List of genes activated by GSC absence. The gene list is sorted by functional grouping, then by fold change of mRNA expression in *glp-1(ts)* relative to wild-type. A fold change cutoff of 4 ($P < 0.05$; n = 1,306) was used (see **Figure 3–figure supplement 1** for rationale). A more conservative fold change cutoff of 5 that captured fewer genes (n = 615) was used for DAVID cluster analysis. CPM denotes counts per million, FC denotes fold change, and FDR denotes false discovery rate.

Supplementary file 1b. List of genes activated by SKN-1 in wild-type animals. The gene list is sorted by functional grouping, then by fold change of mRNA expression in WT *skn-1* RNAi-treated worms relative to WT control vector-treated worms. A fold change cutoff of 0.67 (n = 295) was used to enrich for higher confidence SKN-1 targets. CPM denotes counts per million, FC denotes fold change, and FDR denotes false discovery rate.

Supplementary file 1c. List of genes activated by SKN-1 in GSC(-) animals. The gene list is sorted by functional grouping, then by fold change of mRNA expression in *glp-1(ts) skn-1* RNAi-treated worms relative to *glp-1(ts)* control vector-treated worms. A fold change cutoff of 0.67 ($P < 0.05$; n = 529) was used to enrich for higher confidence SKN-1 targets. CPM denotes counts per million, FC denotes fold change, and FDR denotes false discovery rate.

Supplementary file 1d. List of genes activated by GSC absence in a SKN-1-dependent manner. The gene list is sorted by functional grouping, then by fold change of mRNA expression in *glp-1(ts) skn-1* RNAi-treated worms relative to *glp-1(ts)* control vector-treated worms. We employed a GSC(-) fold change cutoff of > 4 and *skn-1* RNAi cutoff of < 0.67 to generate the list (see **Figure 3–figure supplement 1** for GSC(-) FC cutoff rationale). Statistics were generated by min analysis. Predicted SKN-1 binding sites were determined using 1.5 kb upstream sequences from WBcel235 and the SKN-1 JASPAR matrix (Staab et al., 2013). SKN-1::GFP ChIP-seq binding analysis was performed using the L1, L2, and L3 data sets available from modENCODE (Niu et al., 2011). Additional details are available in **Materials and methods**. CPM denotes counts per million, FC denotes fold change, and FDR denotes false discovery rate.

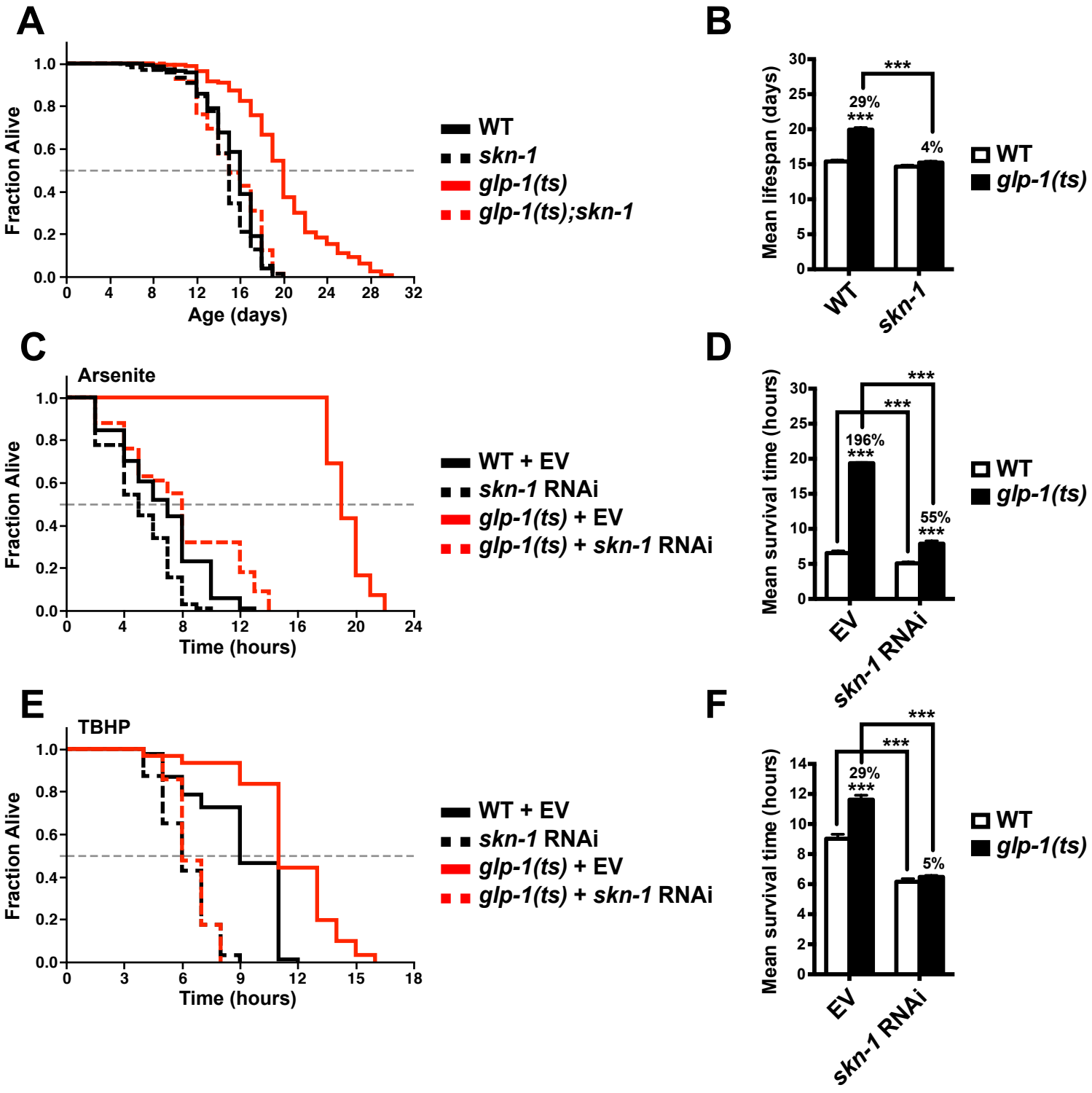
A
Fraction Alive
Age (days)
WT
skn-1
glp-1(ts)
glp-1(ts);skn-1
B
Mean lifespan (days)
29%
***
4%
***
WT
skn-1
WT
glp-1(ts)
C
Arsenite
Fraction Alive
Time (hours)
WT + EV
skn-1 RNAi
glp-1(ts) + EV
glp-1(ts) + skn-1 RNAi
D
Mean survival time (hours)
196%
***
55%
***
***
***
EV
skn-1 RNAi
WT
glp-1(ts)
E
TBHP
Fraction Alive
Time (hours)
WT + EV
skn-1 RNAi
glp-1(ts) + EV
glp-1(ts) + skn-1 RNAi
F
Mean survival time (hours)
29%
***
5%
***
***
EV
skn-1 RNAi
WT
glp-1(ts)

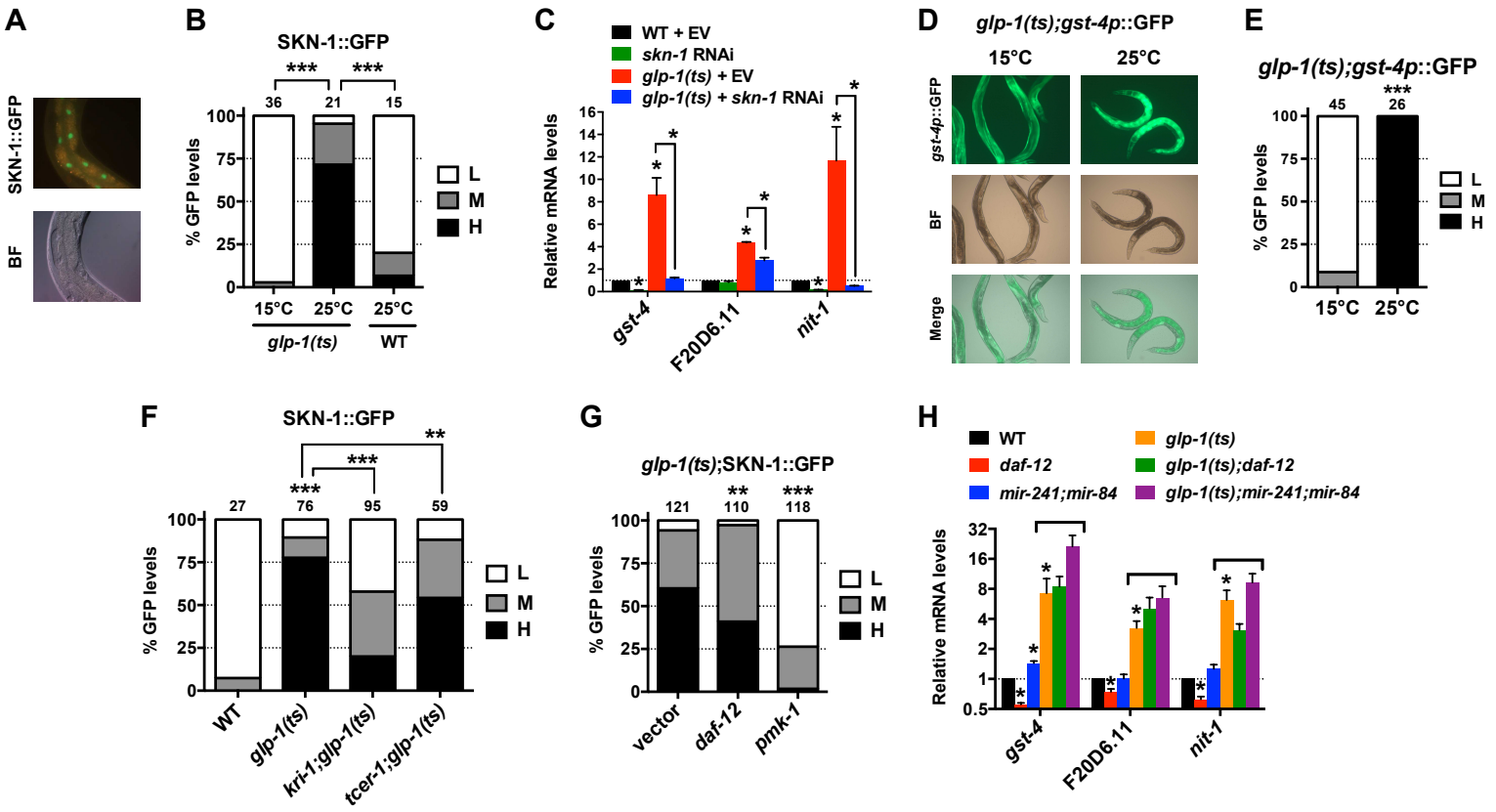
A
SKN-1::GFP
BF
B
SKN-1::GFP
% GFP levels
L
M
H
15°C
25°C
25°C
glp-1(ts)
WT
C
WT + EV
skn-1 RNAi
glp-1(ts) + EV
glp-1(ts) + skn-1 RNAi
Relative mRNA levels
gst-4
F20D6.11
nit-1
D
glp-1(ts);gst-4p::GFP
15°C
25°C
gst-4p::GFP
BF
Merge
E
glp-1(ts);gst-4p::GFP
% GFP levels
15°C
25°C
F
SKN-1::GFP
% GFP levels
WT
glp-1(ts)
kri-1;glp-1(ts)
tcer-1;glp-1(ts)
G
glp-1(ts);SKN-1::GFP
% GFP levels
vector
daf-12
pmk-1
H
WT
daf-12
mir-241;mir-84
glp-1(ts)
glp-1(ts);daf-12
glp-1(ts);mir-241;mir-84
Relative mRNA levels
gst-4
F20D6.11
nit-1

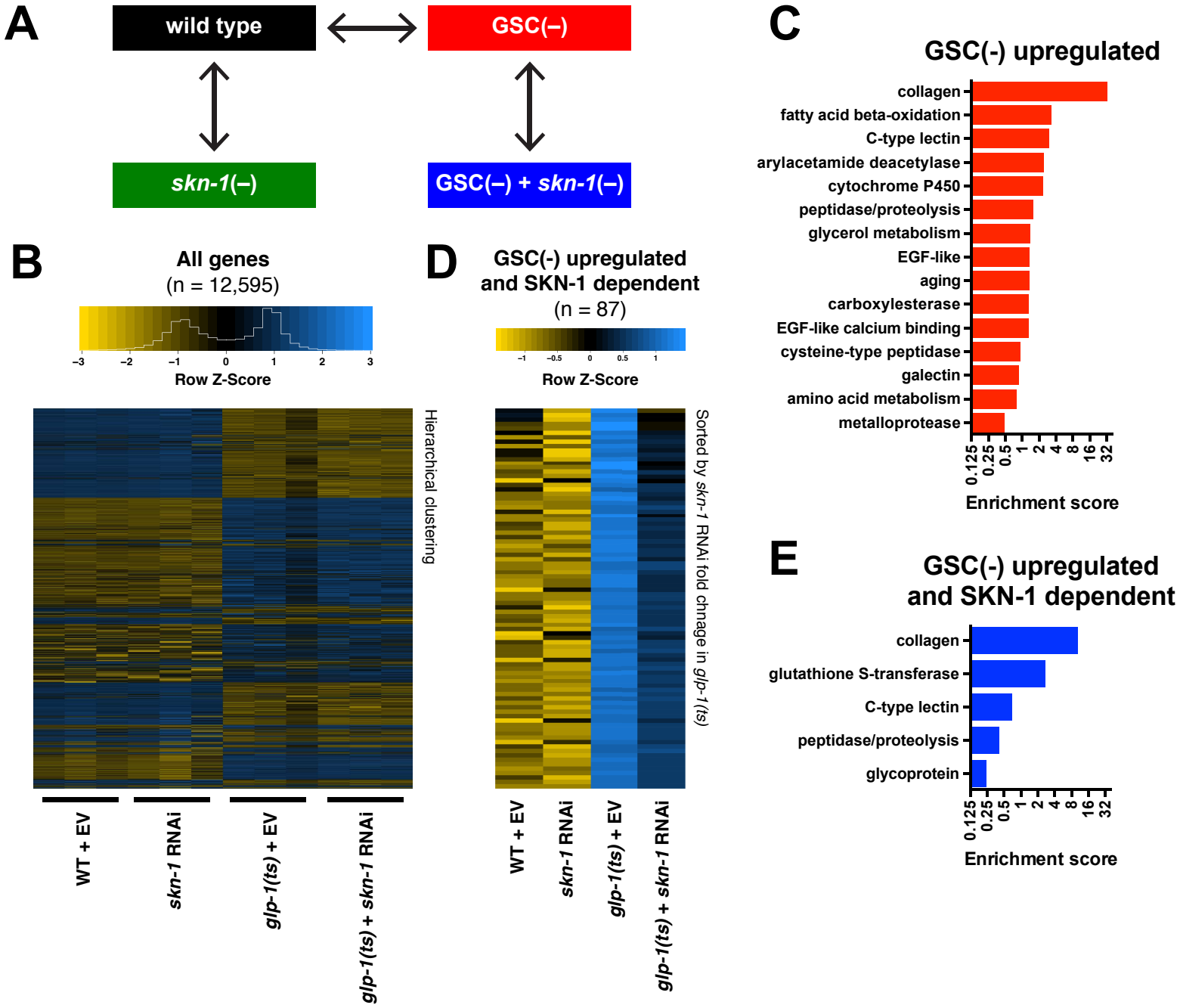
A
wild type
GSC(–)
skn-1(–)
GSC(–) + skn-1(–)
B
All genes
(n = 12,595)
−3 −2 −1 0 1 2 3
Row Z-Score
Hierarchical clustering
WT + EV
skn-1 RNAi
glp-1(ts) + EV
glp-1(ts) + skn-1 RNAi
D
GSC(-) upregulated
and SKN-1 dependent
(n = 87)
−1 −0.5 0 0.5 1
Row Z-Score
Sorted by skn-1 RNAi fold chnage in glp-1(ts)
WT + EV
skn-1 RNAi
glp-1(ts) + EV
glp-1(ts) + skn-1 RNAi
C
GSC(-) upregulated
collagen
fatty acid beta-oxidation
C-type lectin
arylacetamide deacetylase
cytochrome P450
peptidase/proteolysis
glycerol metabolism
EGF-like
aging
carboxylesterase
EGF-like calcium binding
cysteine-type peptidase
galectin
amino acid metabolism
metalloprotease
0.125 0.25 0.5 1 2 4 8 16 32
Enrichment score
E
GSC(-) upregulated
and SKN-1 dependent
collagen
glutathione S-transferase
C-type lectin
peptidase/proteolysis
glycoprotein
0.125 0.25 0.5 1 2 4 8 16 32
Enrichment score

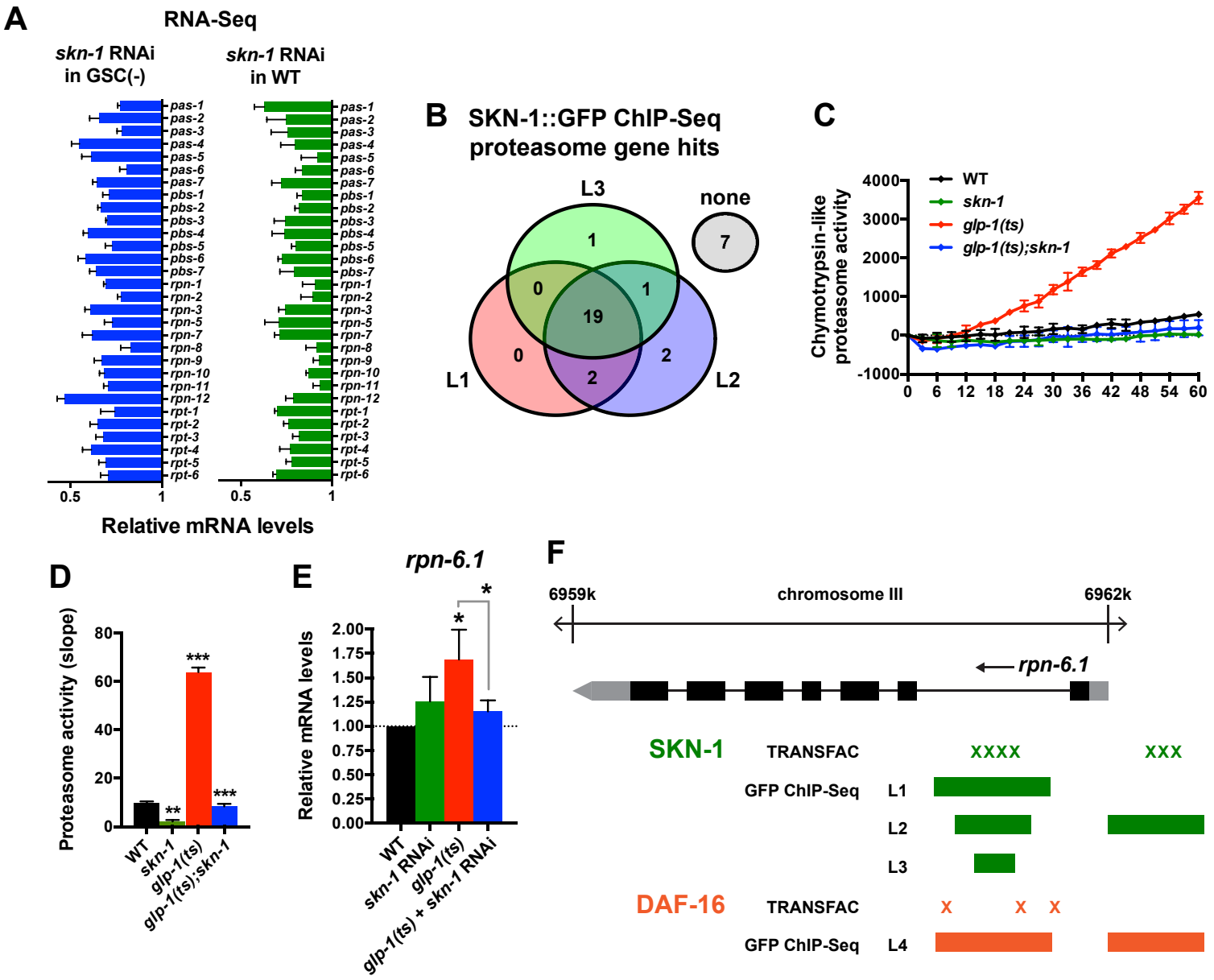
A
RNA-Seq
skn-1 RNAi in GSC(-)
skn-1 RNAi in WT
pas-1
pas-2
pas-3
pas-4
pas-5
pas-6
pas-7
pbs-1
pbs-2
pbs-3
pbs-4
pbs-5
pbs-6
pbs-7
rpn-1
rpn-2
rpn-3
rpn-5
rpn-7
rpn-8
rpn-9
rpn-10
rpn-11
rpn-12
rpt-1
rpt-2
rpt-3
rpt-4
rpt-5
rpt-6
0.5
1
Relative mRNA levels
B
SKN-1::GFP ChIP-Seq
proteasome gene hits
L3
none
L1
L2
1
7
0
1
19
0
2
2
C
Chymotrypsin-like proteasome activity
WT
skn-1
glp-1(ts)
glp-1(ts);skn-1
4000
3000
2000
1000
0
-1000
0
6
12
18
24
30
36
42
48
54
60
D
Proteasome activity (slope)
80
60
40
20
0
***
**
***
WT
skn-1
glp-1(ts)
glp-1(ts);skn-1
E
rpn-6.1
Relative mRNA levels
2.00
1.75
1.50
1.25
1.00
0.75
0.50
0.25
0.00
*
*
WT
skn-1 RNAi
glp-1(ts)
glp-1(ts) + skn-1 RNAi
F
6959k
chromosome III
6962k
rpn-6.1
SKN-1
TRANSFAC
XXXX
XXX
GFP ChIP-Seq
L1
L2
L3
DAF-16
TRANSFAC
X
X
X
GFP ChIP-Seq
L4

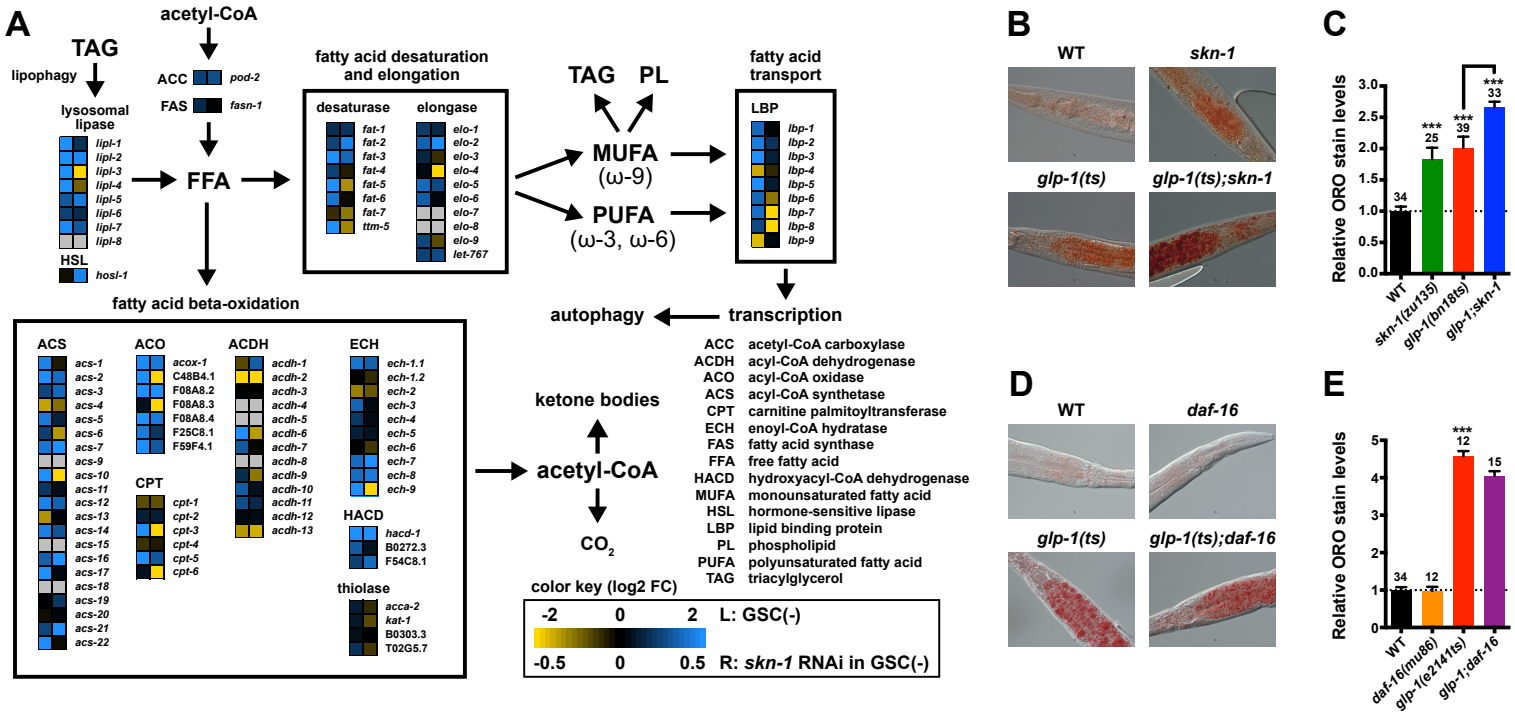
A
TAG
lipophagy
lysosomal lipase
lipl-1
lipl-2
lipl-3
lipl-4
lipl-5
lipl-6
lipl-7
lipl-8
HSL
hosl-1
acetyl-CoA
ACC
pod-2
FAS
fasn-1
FFA
fatty acid desaturation and elongation
desaturase
fat-1
fat-2
fat-3
fat-4
fat-5
fat-6
fat-7
ttm-5
elongase
elo-1
elo-2
elo-3
elo-4
elo-5
elo-6
elo-7
elo-8
elo-9
let-767
TAG PL
MUFA
(ω-9)
PUFA
(ω-3, ω-6)
fatty acid transport
LBP
lbp-1
lbp-2
lbp-3
lbp-4
lbp-5
lbp-6
lbp-7
lbp-8
lbp-9
transcription
autophagy
fatty acid beta-oxidation
ACS
acs-1
acs-2
acs-3
acs-4
acs-5
acs-6
acs-7
acs-9
acs-10
acs-11
acs-12
acs-13
acs-14
acs-15
acs-16
acs-17
acs-18
acs-19
acs-20
acs-21
acs-22
ACO
acox-1
C48B4.1
F08A8.2
F08A8.3
F08A8.4
F25C8.1
F59F4.1
CPT
cpt-1
cpt-2
cpt-3
cpt-4
cpt-5
cpt-6
ACDH
acdh-1
acdh-2
acdh-3
acdh-4
acdh-5
acdh-6
acdh-7
acdh-8
acdh-9
acdh-10
acdh-11
acdh-12
acdh-13
ECH
ech-1.1
ech-1.2
ech-2
ech-3
ech-4
ech-5
ech-6
ech-7
ech-8
ech-9
HACD
hacd-1
B0272.3
F54C8.1
thiolase
acca-2
kat-1
B0303.3
T02G5.7
ketone bodies
acetyl-CoA
CO2
ACC acetyl-CoA carboxylase
ACDH acyl-CoA dehydrogenase
ACO acyl-CoA oxidase
ACS acyl-CoA synthetase
CPT carnitine palmitoyltransferase
ECH enoyl-CoA hydratase
FAS fatty acid synthase
FFA free fatty acid
HACD hydroxyacyl-CoA dehydrogenase
MUFA monounsaturated fatty acid
HSL hormone-sensitive lipase
LBP lipid binding protein
PL phospholipid
PUFA polyunsaturated fatty acid
TAG triacylglycerol
color key (log2 FC)
-2 0 2
L: GSC(-)
-0.5 0 0.5
R: skn-1 RNAi in GSC(-)
B
WT
skn-1
glp-1(ts)
glp-1(ts);skn-1
C
Relative ORO stain levels
3.0
2.5
2.0
1.5
1.0
0.5
0.0
34
***
25
***
39
***
33
WT
skn-1(zu135)
glp-1(bn18ts)
glp-1;skn-1
D
WT
daf-16
glp-1(ts)
glp-1(ts);daf-16
E
Relative ORO stain levels
5
4
3
2
1
0
34
12
***
12
15
WT
daf-16(mu86)
glp-1(e2141ts)
glp-1;daf-16

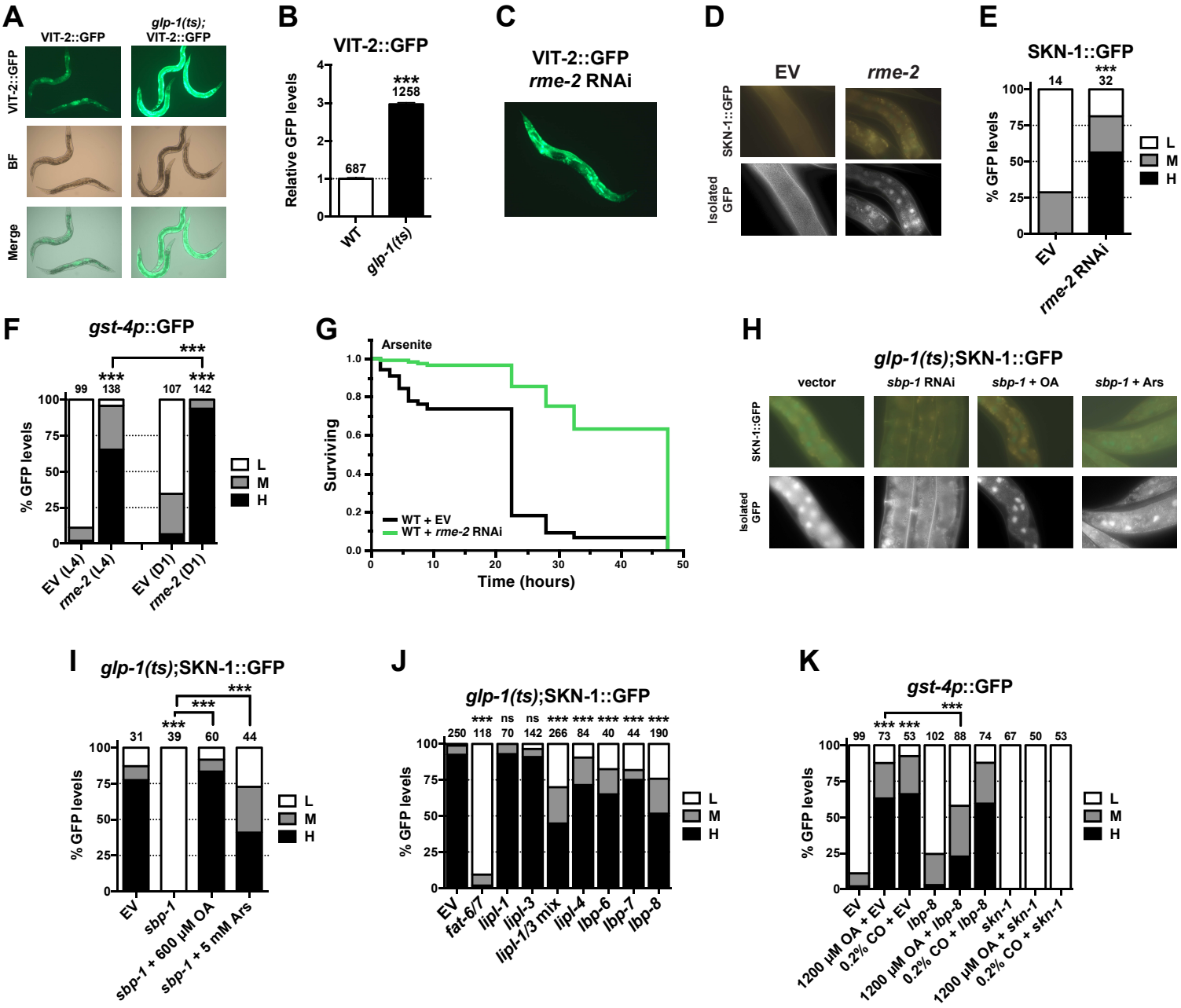
A
VIT-2::GFP
glp-1(ts); VIT-2::GFP
VIT-2::GFP
BF
Merge
B
VIT-2::GFP
Relative GFP levels
***
1258
687
WT
glp-1(ts)
C
VIT-2::GFP
rme-2 RNAi
D
EV
rme-2
SKN-1::GFP
Isolated GFP
E
SKN-1::GFP
% GFP levels
14
***
32
L
M
H
EV
rme-2 RNAi
F
gst-4p::GFP
% GFP levels
99
***
138
107
***
142
***
***
L
M
H
EV (L4)
rme-2 (L4)
EV (D1)
rme-2 (D1)
G
Arsenite
Surviving
WT + EV
WT + rme-2 RNAi
Time (hours)
H
glp-1(ts);SKN-1::GFP
vector
sbp-1 RNAi
sbp-1 + OA
sbp-1 + Ars
SKN-1::GFP
Isolated GFP
I
glp-1(ts);SKN-1::GFP
% GFP levels
31
***
39
***
60
***
44
L
M
H
EV
sbp-1
sbp-1 + 600 µM OA
sbp-1 + 5 mM Ars
J
glp-1(ts);SKN-1::GFP
% GFP levels
250
***
118
ns
70
ns
142
***
266
***
84
***
40
***
44
***
190
L
M
H
EV
fat-6/7
lipl-1
lipl-3
lipl-1/3 mix
lipl-4
lbp-6
lbp-7
lbp-8
K
gst-4p::GFP
% GFP levels
99
***
73
***
53
102
88
74
67
50
53
***
L
M
H
EV
1200 µM OA + EV
0.2% CO + EV
lbp-8
1200 µM OA + lbp-8
0.2% CO + lbp-8
skn-1
1200 µM OA + skn-1
0.2% CO + skn-1

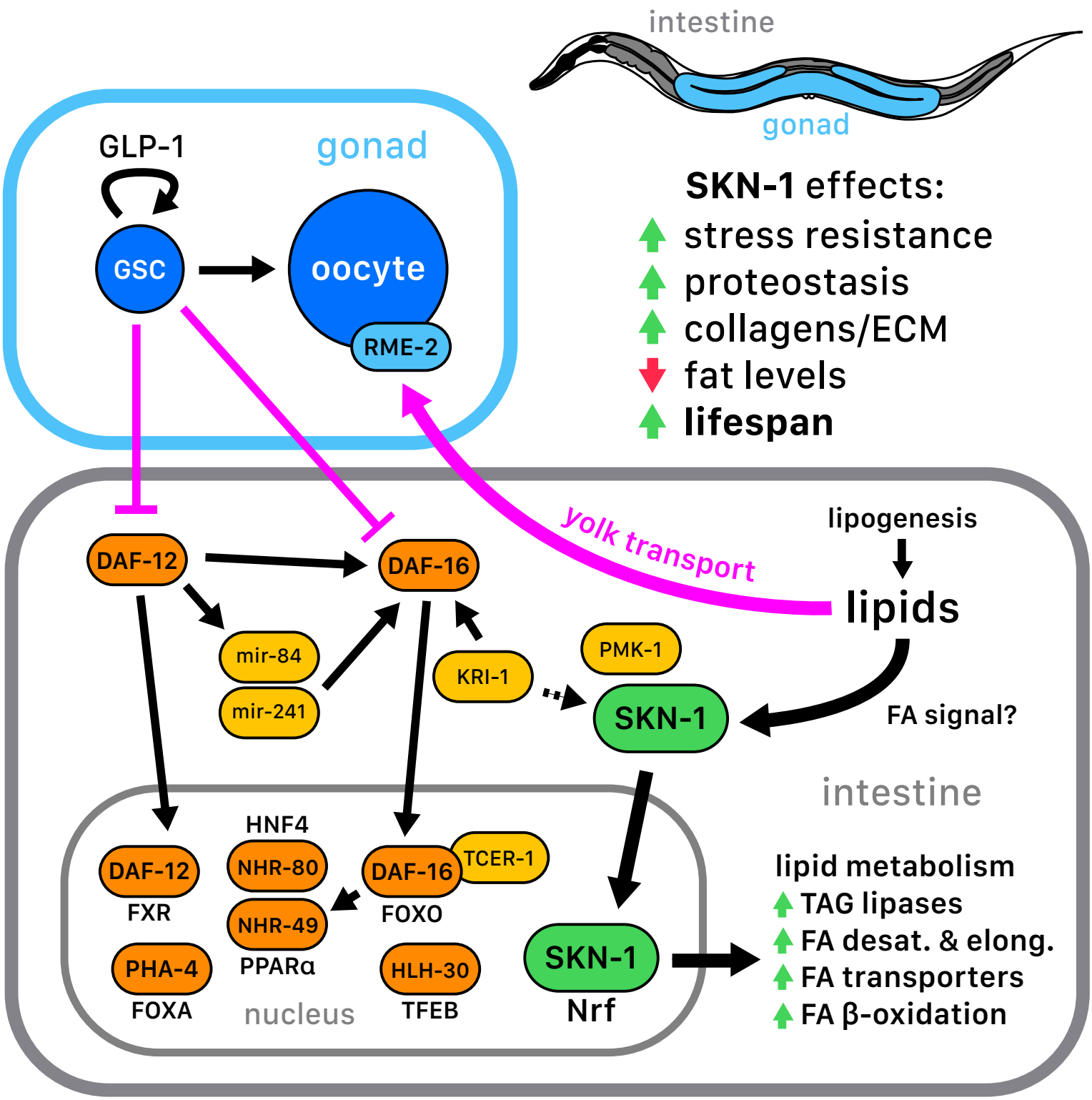
intestine
gonad
GLP-1
gonad
GSC
oocyte
RME-2
SKN-1 effects:
stress resistance
proteostasis
collagens/ECM
fat levels
lifespan
yolk transport
lipogenesis
lipids
DAF-12
DAF-16
mir-84
mir-241
KRI-1
PMK-1
SKN-1
FA signal?
intestine
HNF4
DAF-12
FXR
NHR-80
NHR-49
PPARα
DAF-16
FOXO
TCER-1
PHA-4
FOXA
HLH-30
TFEB
nucleus
SKN-1
Nrf
lipid metabolism
TAG lipases
FA desat. & elong.
FA transporters
FA β-oxidation